

**Measurement of $e^+e^- \rightarrow \eta J/\psi$ cross section
from $\sqrt{s} = 3.808$ GeV to 4.951 GeV**

M. Ablikim,¹ M. N. Achasov,^{4,b} P. Adlarson,⁷⁵ X. C. Ai,⁸¹ R. Aliberti,³⁵ A. Amoroso,^{74a,74c} M. R. An,³⁹ Q. An,^{71,58} Y. Bai,⁵⁷ O. Bakina,³⁶ I. Balossino,^{29a} Y. Ban,^{46,g} H.-R. Bao,⁶³ V. Batozskaya,^{1,44} K. Begzsuren,³² N. Berger,³⁵ M. Berlowski,⁴⁴ M. Bertani,^{28a} D. Bettoni,^{29a} F. Bianchi,^{74a,74c} E. Bianco,^{74a,74c} A. Bortone,^{74a,74c} I. Boyko,³⁶ R. A. Briere,⁵ A. Brueggemann,⁶⁸ H. Cai,⁷⁶ X. Cai,^{1,58} A. Calcaterra,^{28a} G. F. Cao,^{1,63} N. Cao,^{1,63} S. A. Cetin,^{62a} J. F. Chang,^{1,58} T. T. Chang,⁷⁷ W. L. Chang,^{1,63} G. R. Che,⁴³ G. Chelkov,^{36,a} C. Chen,⁴³ Chao Chen,⁵⁵ G. Chen,¹ H. S. Chen,^{1,63} M. L. Chen,^{1,58,63} S. J. Chen,⁴² S. L. Chen,⁴⁵ S. M. Chen,⁶¹ T. Chen,^{1,63} X. R. Chen,^{31,63} X. T. Chen,^{1,63} Y. B. Chen,^{1,58} Y. Q. Chen,³⁴ Z. J. Chen,^{25,h} S. K. Choi,¹⁰ X. Chu,⁴³ G. Cibinetto,^{29a} S. C. Coen,³ F. Cossio,^{74c} J. J. Cui,⁵⁰ H. L. Dai,^{1,58} J. P. Dai,⁷⁹ A. Dbeysy, R. E. de Boer,³ D. Dedovich,³⁶ Z. Y. Deng,¹ A. Denig,³⁵ I. Denysenko,³⁶ M. Destefanis,^{74a,74c} F. De Mori,^{74a,74c} B. Ding,^{66,1} X. X. Ding,^{46,g} Y. Ding,⁴⁰ Y. Ding,³⁴ J. Dong,^{1,58} L. Y. Dong,^{1,63} M. Y. Dong,^{1,58,63} X. Dong,⁷⁶ M. C. Du,¹ S. X. Du,⁸¹ Z. H. Duan,⁴² P. Egorov,^{36,a} Y. H. Fan,⁴⁵ J. Fang,^{1,58} S. S. Fang,^{1,63} W. X. Fang,¹ Y. Fang,¹ Y. Q. Fang,^{1,58} R. Farinelli,^{29a} L. Fava,^{74b,74c} F. Feldbauer,³ G. Felici,^{28a} C. Q. Feng,^{71,58} J. H. Feng,⁵⁹ Y. T. Feng,^{71,58} K. Fischer,⁶⁹ M. Fritsch,³ C. D. Fu,¹ J. L. Fu,⁶³ Y. W. Fu,¹ H. Gao,⁶³ Y. N. Gao,^{46,g} Yang Gao,^{71,58} S. Garbolino,^{74c} I. Garzia,^{29a,29b} P. T. Ge,⁷⁶ Z. W. Ge,⁴² C. Geng,⁵⁹ E. M. Gersabeck,⁶⁷ A. Gilman,⁶⁹ K. Goetzen,¹³ L. Gong,⁴⁰ W. X. Gong,^{1,58} W. Gradl,³⁵ S. Gramigna,^{29a,29b} M. Greco,^{74a,74c} M. H. Gu,^{1,58} Y. T. Gu,¹⁵ C. Y. Guan,^{1,63} Z. L. Guan,²² A. Q. Guo,^{31,63} L. B. Guo,⁴¹ M. J. Guo,⁵⁰ R. P. Guo,⁴⁹ Y. P. Guo,^{12,f} A. Guskov,^{36,a} J. Gutierrez,²⁷ T. T. Han,¹ W. Y. Han,³⁹ X. Q. Hao,¹⁹ F. A. Harris,⁶⁵ K. K. He,⁵⁵ K. L. He,^{1,63} F. H. H. Heinsius,³ C. H. Heinz,³⁵ Y. K. Heng,^{1,58,63} C. Herold,⁶⁰ T. Holtmann,³ P. C. Hong,^{12,f} G. Y. Hou,^{1,63} X. T. Hou,^{1,63} Y. R. Hou,⁶³ Z. L. Hou,¹ B. Y. Hu,⁵⁹ H. M. Hu,^{1,63} J. F. Hu,^{56,i} T. Hu,^{1,58,63} Y. Hu,¹ G. S. Huang,^{71,58} K. X. Huang,⁵⁹ L. Q. Huang,^{31,63} X. T. Huang,⁵⁰ Y. P. Huang,¹ T. Hussain,⁷³ N. Hüsken,^{27,35} N. in der Wiesche,⁶⁸ M. Irshad,^{71,58} J. Jackson,²⁷ S. Jaeger,³ S. Janchiv,³² J. H. Jeong,¹⁰ Q. Ji,¹ Q. P. Ji,¹⁹ X. B. Ji,^{1,63} X. L. Ji,^{1,58} Y. Y. Ji,⁵⁰ X. Q. Jia,⁵⁰ Z. K. Jia,^{71,58} H. J. Jiang,⁷⁶ P. C. Jiang,^{46,g} S. S. Jiang,³⁹ T. J. Jiang,¹⁶ X. S. Jiang,^{1,58,63} Y. Jiang,⁶³ J. B. Jiao,⁵⁰ Z. Jiao,²³ S. Jin,⁴² Y. Jin,⁶⁶ M. Q. Jing,^{1,63} X. M. Jing,⁶³ T. Johansson,⁷⁵ X. K.,¹ S. Kabana,³³ N. Kalantar-Nayestanaki,⁶⁴ X. L. Kang,⁹ X. S. Kang,⁴⁰ M. Kavatsyuk,⁶⁴ B. C. Ke,⁸¹ V. Khachatryan,²⁷ A. Khoukaz,⁶⁸ R. Kiuchi,¹ R. Kliemt,¹³ O. B. Kolcu,^{62a} B. Kopf,³ M. Kuessner,³ A. Kupsc,^{44,75} W. Kühn,³⁷ J. J. Lane,⁶⁷ P. Larin,¹⁸ A. Lavanaia,²⁶ L. Lavezzi,^{74a,74c} T. T. Lei,^{71,58} Z. H. Lei,^{71,58} H. Leithoff,³⁵ M. Lellmann,³⁵ T. Lenz,³⁵ C. Li,⁴⁷ C. Li,⁴³ C. H. Li,³⁹ Cheng Li,^{71,58} D. M. Li,⁸¹ F. Li,^{1,58} G. Li,¹ H. Li,^{71,58} H. B. Li,^{1,63} H. J. Li,¹⁹ H. N. Li,^{56,i} Hui Li,⁴³ J. R. Li,⁶¹ J. S. Li,⁵⁹ J. W. Li,⁵⁰ Ke Li,¹ L. J. Li,^{1,63} L. K. Li,¹ Lei Li,⁴⁸ M. H. Li,⁴³ P. R. Li,^{38,k} Q. X. Li,⁵⁰ S. X. Li,¹² T. Li,⁵⁰ W. D. Li,^{1,63} W. G. Li,¹ X. H. Li,^{71,58} X. L. Li,⁵⁰ Xiaoyu Li,^{1,63} Y. G. Li,^{46,g} Z. J. Li,⁵⁹ Z. X. Li,¹⁵ C. Liang,⁴² H. Liang,^{71,58} H. Liang,^{1,63} Y. F. Liang,⁵⁴ Y. T. Liang,^{31,63} G. R. Liao,¹⁴ L. Z. Liao,⁵⁰ Y. P. Liao,^{1,63} J. Libby,²⁶ A. Limphirat,⁶⁰ D. X. Lin,^{31,63} T. Lin,¹ B. J. Liu,¹ B. X. Liu,⁷⁶ C. Liu,³⁴ C. X. Liu,¹ F. H. Liu,⁵³ Fang Liu,¹ Feng Liu,⁶ G. M. Liu,^{56,i} H. Liu,^{38,j,k} H. B. Liu,¹⁵ H. M. Liu,^{1,63} Huanhuan Liu,¹ Huihui Liu,²¹ J. B. Liu,^{71,58} J. Y. Liu,^{1,63} K. Liu,¹ K. Y. Liu,⁴⁰ Ke Liu,²² L. Liu,^{71,58} L. C. Liu,⁴³ Lu Liu,⁴³ M. H. Liu,^{12,f} P. L. Liu,¹ Q. Liu,⁶³ S. B. Liu,^{71,58} T. Liu,^{12,f} W. K. Liu,⁴³ W. M. Liu,^{71,58} X. Liu,^{38,j,k} Y. Liu,⁸¹ Y. Liu,^{38,j,k} Y. B. Liu,⁴³ Z. A. Liu,^{1,58,63} Z. Q. Liu,⁵⁰ X. C. Lou,^{1,58,63} F. X. Lu,⁵⁹ H. J. Lu,²³ J. G. Lu,^{1,58} X. L. Lu,¹ Y. Lu,⁷ Y. P. Lu,^{1,58} Z. H. Lu,^{1,63} C. L. Luo,⁴¹ M. X. Luo,⁸⁰ T. Luo,^{12,f} X. L. Luo,^{1,58} X. R. Lyu,⁶³ Y. F. Lyu,⁴³ F. C. Ma,⁴⁰ H. Ma,⁷⁹ H. L. Ma,¹ J. L. Ma,^{1,63} L. L. Ma,⁵⁰ M. M. Ma,^{1,63} Q. M. Ma,¹ R. Q. Ma,^{1,63} X. Y. Ma,^{1,58} Y. Ma,^{46,g} Y. M. Ma,³¹ F. E. Maas,¹⁸ M. Maggiora,^{74a,74c} S. Malde,⁶⁹ Q. A. Malik,⁷³ A. Mangoni,^{28b} Y. J. Mao,^{46,g} Z. P. Mao,¹ S. Marcello,^{74a,74c} Z. X. Meng,⁶⁶ J. G. Messchendorp,^{13,64} G. Mezzadri,^{29a} H. Miao,^{1,63} T. J. Min,⁴² R. E. Mitchell,²⁷ X. H. Mo,^{1,58,63} B. Moses,²⁷ N. Yu. Muchnoi,^{4,b} J. Muskalla,³⁵ Y. Nefedov,³⁶ F. Nerling,^{18,d} I. B. Nikolaev,^{4,b} Z. Ning,^{1,58} S. Nisar,^{11,1} Q. L. Niu,^{38,j,k} W. D. Niu,⁵⁵ Y. Niu,⁵⁰ S. L. Olsen,⁶³ Q. Ouyang,^{1,58,63} S. Pacetti,^{28b,28c} X. Pan,⁵⁵ Y. Pan,⁵⁷ A. Pathak,³⁴ P. Patteri,^{28a} Y. P. Pei,^{71,58} M. Pelizaeus,³ H. P. Peng,^{71,58} Y. Y. Peng,^{38,j,k} K. Peters,^{13,d} J. L. Ping,⁴¹ R. G. Ping,^{1,63} S. Plura,³⁵ V. Prasad,³³ F. Z. Qi,¹ H. Qi,^{71,58} H. R. Qi,⁶¹ M. Qi,⁴² T. Y. Qi,^{12,f} S. Qian,^{1,58} W. B. Qian,⁶³ C. F. Qiao,⁶³ J. J. Qin,⁷² L. Q. Qin,¹⁴ X. S. Qin,⁵⁰ Z. H. Qin,^{1,58} J. F. Qiu,¹ S. Q. Qu,⁶¹ C. F. Redmer,³⁵ K. J. Ren,³⁹ A. Rivetti,^{74c} M. Rolo,^{74c} G. Rong,^{1,63} Ch. Rosner,¹⁸ S. N. Ruan,⁴³ N. Salone,⁴⁴ A. Sarantsev,^{36,c} Y. Schelhaas,³⁵ K. Schoenning,⁷⁵ M. Scodreggio,^{29a,29b} K. Y. Shan,^{12,f} W. Shan,²⁴ X. Y. Shan,^{71,58} J. F. Shangguan,⁵⁵ L. G. Shao,^{1,63} M. Shao,^{71,58} C. P. Shen,^{12,f} H. F. Shen,^{1,63} W. H. Shen,⁶³ X. Y. Shen,^{1,63} B. A. Shi,⁶³ H. C. Shi,^{71,58} J. L. Shi,¹² J. Y. Shi,¹ Q. Q. Shi,⁵⁵ R. S. Shi,^{1,63} X. Shi,^{1,58} J. J. Song,¹⁹ T. Z. Song,⁵⁹ W. M. Song,^{34,1} Y. J. Song,¹² Y. X. Song,^{46,g} S. Sosio,^{74a,74c} S. Spataro,^{74a,74c} F. Stieler,³⁵ Y. J. Su,⁶⁵ G. B. Sun,⁷⁶ G. X. Sun,¹ H. Sun,⁶³ H. K. Sun,¹ J. F. Sun,¹⁹ K. Sun,⁶¹ L. Sun,⁷⁶ S. S. Sun,^{1,63} T. Sun,^{51,e} W. Y. Sun,³⁴ Y. Sun,⁹ Y. J. Sun,^{71,58} Y. Z. Sun,¹ Z. T. Sun,⁵⁰ Y. X. Tan,^{71,58} C. J. Tang,⁵⁴ G. Y. Tang,¹ J. Tang,⁵⁹ Y. A. Tang,⁷⁶ L. Y. Tao,⁷² Q. T. Tao,^{25,h} M. Tat,⁶⁹ J. X. Teng,^{71,58} V. Thoren,⁷⁵ W. H. Tian,⁵² W. H. Tian,⁵⁹ Y. Tian,^{31,63} Z. F. Tian,⁷⁶ I. Uman,^{62b} Y. Wan,⁵⁵ S. J. Wang,⁵⁰ B. Wang,¹ B. L. Wang,⁶³ Bo Wang,^{71,58} C. W. Wang,⁴² D. Y. Wang,^{46,g} F. Wang,⁷² H. J. Wang,^{38,j,k} J. P. Wang,⁵⁰ K. Wang,^{1,58}

L. L. Wang,¹ M. Wang,⁵⁰ Meng Wang,^{1,63} N. Y. Wang,⁶³ S. Wang,^{12,f} S. Wang,^{38,j,k} T. Wang,^{12,f} T. J. Wang,⁴³ W. Wang,⁷² W. Wang,⁵⁹ W. P. Wang,^{71,58} X. Wang,^{46,g} X. F. Wang,^{38,j,k} X. J. Wang,³⁹ X. L. Wang,^{12,f} Y. Wang,⁶¹ Y. D. Wang,⁴⁵ Y. F. Wang,^{1,58,63} Y. L. Wang,¹⁹ Y. N. Wang,⁴⁵ Y. Q. Wang,¹ Yaqian Wang,^{17,1} Yi Wang,⁶¹ Z. Wang,^{1,58} Z. L. Wang,⁷² Z. Y. Wang,^{1,63} Ziyi Wang,⁶³ D. Wei,⁷⁰ D. H. Wei,¹⁴ F. Weidner,⁶⁸ S. P. Wen,¹ C. W. Wenzel,³ U. Wiedner,³ G. Wilkinson,⁶⁹ M. Wolke,⁷⁵ L. Wollenberg,³ C. Wu,³⁹ J. F. Wu,^{1,8} L. H. Wu,¹ L. J. Wu,^{1,63} X. Wu,^{12,f} X. H. Wu,³⁴ Y. Wu,⁷¹ Y. H. Wu,⁵⁵ Y. J. Wu,³¹ Z. Wu,^{1,58} L. Xia,^{71,58} X. M. Xian,³⁹ T. Xiang,^{46,g} D. Xiao,^{38,j,k} G. Y. Xiao,⁴² S. Y. Xiao,¹ Y. L. Xiao,^{12,f} Z. J. Xiao,⁴¹ C. Xie,⁴² X. H. Xie,^{46,g} Y. Xie,⁵⁰ Y. G. Xie,^{1,58} Y. H. Xie,⁶ Z. P. Xie,^{71,58} T. Y. Xing,^{1,63} C. F. Xu,^{1,63} C. J. Xu,⁵⁹ G. F. Xu,¹ H. Y. Xu,⁶⁶ Q. J. Xu,¹⁶ Q. N. Xu,³⁰ W. Xu,¹ W. L. Xu,⁶⁶ X. P. Xu,⁵⁵ Y. C. Xu,⁷⁸ Z. P. Xu,⁴² Z. S. Xu,⁶³ F. Yan,^{12,f} L. Yan,^{12,f} W. B. Yan,^{71,58} W. C. Yan,⁸¹ X. Q. Yan,¹ H. J. Yang,^{51,e} H. L. Yang,³⁴ H. X. Yang,¹ Tao Yang,¹ Y. Yang,^{12,f} Y. F. Yang,⁴³ Y. X. Yang,^{1,63} Yifan Yang,^{1,63} Z. W. Yang,^{38,j,k} Z. P. Yao,⁵⁰ M. Ye,^{1,58} M. H. Ye,⁸ J. H. Yin,¹ Z. Y. You,⁵⁹ B. X. Yu,^{1,58,63} C. X. Yu,⁴³ G. Yu,^{1,63} J. S. Yu,^{25,h} T. Yu,⁷² X. D. Yu,^{46,g} C. Z. Yuan,^{1,63} L. Yuan,² S. C. Yuan,¹ Y. Yuan,^{1,63} Z. Y. Yuan,⁵⁹ C. X. Yue,³⁹ A. A. Zafar,⁷³ F. R. Zeng,⁵⁰ S. H. Zeng,⁷² X. Zeng,^{12,f} Y. Zeng,^{25,h} Y. J. Zeng,^{1,63} X. Y. Zhai,³⁴ Y. C. Zhai,⁵⁰ Y. H. Zhan,⁵⁹ A. Q. Zhang,^{1,63} B. L. Zhang,^{1,63} B. X. Zhang,¹ D. H. Zhang,⁴³ G. Y. Zhang,¹⁹ H. Zhang,⁷¹ H. C. Zhang,^{1,58,63} H. H. Zhang,⁵⁹ H. H. Zhang,³⁴ H. Q. Zhang,^{1,58,63} H. Y. Zhang,^{1,58} J. Zhang,⁸¹ J. Zhang,⁵⁹ J. J. Zhang,⁵² J. L. Zhang,²⁰ J. Q. Zhang,⁴¹ J. W. Zhang,^{1,58,63} J. X. Zhang,^{38,j,k} J. Y. Zhang,¹ J. Z. Zhang,^{1,63} Jianyu Zhang,⁶³ L. M. Zhang,⁶¹ L. Q. Zhang,⁵⁹ Lei Zhang,⁴² P. Zhang,^{1,63} Q. Y. Zhang,^{39,81} Shuihan Zhang,^{1,63} Shulei Zhang,^{25,h} X. D. Zhang,⁴⁵ X. M. Zhang,¹ X. Y. Zhang,⁵⁰ Y. Zhang,⁶⁹ Y. Zhang,⁷² Y. T. Zhang,⁸¹ Y. H. Zhang,^{1,58} Yan Zhang,^{71,58} Yao Zhang,¹ Z. D. Zhang,¹ Z. H. Zhang,¹ Z. L. Zhang,³⁴ Z. Y. Zhang,⁴³ Z. Y. Zhang,⁷⁶ G. Zhao,¹ J. Y. Zhao,^{1,63} J. Z. Zhao,^{1,58} Lei Zhao,^{71,58} Ling Zhao,¹ M. G. Zhao,⁴³ R. P. Zhao,⁶³ S. J. Zhao,⁸¹ Y. B. Zhao,^{1,58} Y. X. Zhao,^{31,63} Z. G. Zhao,^{71,58} A. Zhemchugov,^{36,a} B. Zheng,⁷² J. P. Zheng,^{1,58} W. J. Zheng,^{1,63} Y. H. Zheng,⁶³ B. Zhong,⁴¹ X. Zhong,⁵⁹ H. Zhou,⁵⁰ L. P. Zhou,^{1,63} X. Zhou,⁷⁶ X. K. Zhou,⁶ X. R. Zhou,^{71,58} X. Y. Zhou,³⁹ Y. Z. Zhou,^{12,f} J. Zhu,⁴³ K. Zhu,¹ K. J. Zhu,^{1,58,63} L. Zhu,³⁴ L. X. Zhu,⁶³ S. H. Zhu,⁷⁰ S. Q. Zhu,⁴² T. J. Zhu,^{12,f} W. J. Zhu,^{12,f} Y. C. Zhu,^{71,58} Z. A. Zhu,^{1,63} J. H. Zou,¹ and J. Zu^{71,58}

(BESIII Collaboration)

¹*Institute of High Energy Physics, Beijing 100049, People's Republic of China*²*Beihang University, Beijing 100191, People's Republic of China*³*Bochum Ruhr-University, D-44780 Bochum, Germany*⁴*Budker Institute of Nuclear Physics SB RAS (BINP), Novosibirsk 630090, Russia*⁵*Carnegie Mellon University, Pittsburgh, Pennsylvania 15213, USA*⁶*Central China Normal University, Wuhan 430079, People's Republic of China*⁷*Central South University, Changsha 410083, People's Republic of China*⁸*China Center of Advanced Science and Technology, Beijing 100190, People's Republic of China*⁹*China University of Geosciences, Wuhan 430074, People's Republic of China*¹⁰*Chung-Ang University, Seoul 06974, Republic of Korea*¹¹*COMSATS University Islamabad, Lahore Campus, Defence Road, Off Raiwind Road, 54000 Lahore, Pakistan*¹²*Fudan University, Shanghai 200433, People's Republic of China*¹³*GSI Helmholtzcentre for Heavy Ion Research GmbH, D-64291 Darmstadt, Germany*¹⁴*Guangxi Normal University, Guilin 541004, People's Republic of China*¹⁵*Guangxi University, Nanning 530004, People's Republic of China*¹⁶*Hangzhou Normal University, Hangzhou 310036, People's Republic of China*¹⁷*Hebei University, Baoding 071002, People's Republic of China*¹⁸*Helmholtz Institute Mainz, Staudinger Weg 18, D-55099 Mainz, Germany*¹⁹*Henan Normal University, Xinxiang 453007, People's Republic of China*²⁰*Henan University, Kaifeng 475004, People's Republic of China*²¹*Henan University of Science and Technology, Luoyang 471003, People's Republic of China*²²*Henan University of Technology, Zhengzhou 450001, People's Republic of China*²³*Huangshan College, Huangshan 245000, People's Republic of China*²⁴*Hunan Normal University, Changsha 410081, People's Republic of China*²⁵*Hunan University, Changsha 410082, People's Republic of China*²⁶*Indian Institute of Technology Madras, Chennai 600036, India*²⁷*Indiana University, Bloomington, Indiana 47405, USA*^{28a}*INFN Laboratori Nazionali di Frascati, I-00044 Frascati, Italy*^{28b}*INFN Sezione di Perugia, I-06100 Perugia, Italy*

- ^{28c}University of Perugia, I-06100 Perugia, Italy
- ^{29a}INFN Sezione di Ferrara, I-44122 Ferrara, Italy
- ^{29b}University of Ferrara, I-44122 Ferrara, Italy
- ³⁰Inner Mongolia University, Hohhot 010021, People's Republic of China
- ³¹Institute of Modern Physics, Lanzhou 730000, People's Republic of China
- ³²Institute of Physics and Technology, Peace Avenue 54B, Ulaanbaatar 13330, Mongolia
- ³³Instituto de Alta Investigación, Universidad de Tarapacá, Casilla 7D, Arica 1000000, Chile
- ³⁴Jilin University, Changchun 130012, People's Republic of China
- ³⁵Johannes Gutenberg University of Mainz, Johann-Joachim-Becher-Weg 45, D-55099 Mainz, Germany
- ³⁶Joint Institute for Nuclear Research, 141980 Dubna, Moscow region, Russia
- ³⁷Justus-Liebig-Universität Giessen, II. Physikalisches Institut, Heinrich-Buff-Ring 16, D-35392 Giessen, Germany
- ³⁸Lanzhou University, Lanzhou 730000, People's Republic of China
- ³⁹Liaoning Normal University, Dalian 116029, People's Republic of China
- ⁴⁰Liaoning University, Shenyang 110036, People's Republic of China
- ⁴¹Nanjing Normal University, Nanjing 210023, People's Republic of China
- ⁴²Nanjing University, Nanjing 210093, People's Republic of China
- ⁴³Nankai University, Tianjin 300071, People's Republic of China
- ⁴⁴National Centre for Nuclear Research, Warsaw 02-093, Poland
- ⁴⁵North China Electric Power University, Beijing 102206, People's Republic of China
- ⁴⁶Peking University, Beijing 100871, People's Republic of China
- ⁴⁷Qufu Normal University, Qufu 273165, People's Republic of China
- ⁴⁸Renmin University of China, Beijing 100872, People's Republic of China
- ⁴⁹Shandong Normal University, Jinan 250014, People's Republic of China
- ⁵⁰Shandong University, Jinan 250100, People's Republic of China
- ⁵¹Shanghai Jiao Tong University, Shanghai 200240, People's Republic of China
- ⁵²Shanxi Normal University, Linfen 041004, People's Republic of China
- ⁵³Shanxi University, Taiyuan 030006, People's Republic of China
- ⁵⁴Sichuan University, Chengdu 610064, People's Republic of China
- ⁵⁵Soochow University, Suzhou 215006, People's Republic of China
- ⁵⁶South China Normal University, Guangzhou 510006, People's Republic of China
- ⁵⁷Southeast University, Nanjing 211100, People's Republic of China
- ⁵⁸State Key Laboratory of Particle Detection and Electronics, Beijing 100049, Hefei 230026, People's Republic of China
- ⁵⁹Sun Yat-Sen University, Guangzhou 510275, People's Republic of China
- ⁶⁰Suranaree University of Technology, University Avenue 111, Nakhon Ratchasima 30000, Thailand
- ⁶¹Tsinghua University, Beijing 100084, People's Republic of China
- ^{62a}Turkish Accelerator Center Particle Factory Group, Istinye University, 34010, Istanbul, Turkey
- ^{62b}Near East University, Nicosia, North Cyprus, 99138, Mersin 10, Turkey
- ⁶³University of Chinese Academy of Sciences, Beijing 100049, People's Republic of China
- ⁶⁴University of Groningen, NL-9747 AA Groningen, The Netherlands
- ⁶⁵University of Hawaii, Honolulu, Hawaii 96822, USA
- ⁶⁶University of Jinan, Jinan 250022, People's Republic of China
- ⁶⁷University of Manchester, Oxford Road, Manchester, M13 9PL, United Kingdom
- ⁶⁸University of Muenster, Wilhelm-Klemm-Strasse 9, 48149 Muenster, Germany
- ⁶⁹University of Oxford, Keble Road, Oxford OX13RH, United Kingdom
- ⁷⁰University of Science and Technology Liaoning, Anshan 114051, People's Republic of China
- ⁷¹University of Science and Technology of China, Hefei 230026, People's Republic of China
- ⁷²University of South China, Hengyang 421001, People's Republic of China
- ⁷³University of the Punjab, Lahore-54590, Pakistan
- ^{74a}University of Turin and INFN, University of Turin, I-10125 Turin, Italy
- ^{74b}University of Eastern Piedmont, I-15121 Alessandria, Italy
- ^{74c}INFN, I-10125 Turin, Italy
- ⁷⁵Uppsala University, Box 516, SE-75120 Uppsala, Sweden
- ⁷⁶Wuhan University, Wuhan 430072, People's Republic of China
- ⁷⁷Xinyang Normal University, Xinyang 464000, People's Republic of China
- ⁷⁸Yantai University, Yantai 264005, People's Republic of China
- ⁷⁹Yunnan University, Kunming 650500, People's Republic of China

⁸⁰Zhejiang University, Hangzhou 310027, People's Republic of China
⁸¹Zhengzhou University, Zhengzhou 450001, People's Republic of China



(Received 6 October 2023; accepted 6 May 2024; published 29 May 2024)

Using data samples with an integrated luminosity of 22.42 fb^{-1} collected by the BESIII detector operating at the BEPCII storage ring, we measure the cross sections of the $e^+e^- \rightarrow \eta J/\psi$ process at center-of-mass energies from 3.808 to 4.951 GeV. Three structures are observed in the line shape of the measured cross sections. A maximum-likelihood fit with $\psi(4040)$, two additional resonances, and a nonresonant component are performed. The mass and width of the first additional state are $(4219.7 \pm 2.5 \pm 4.5) \text{ MeV}/c^2$ and $(80.7 \pm 4.4 \pm 1.4) \text{ MeV}$, respectively, consistent with the $\psi(4230)$. For the second state, the mass and width are $(4386 \pm 13 \pm 17) \text{ MeV}/c^2$ and $(177 \pm 32 \pm 13) \text{ MeV}$, respectively, consistent with the $\psi(4360)$. The first uncertainties are statistical, and the second ones are systematic. The statistical significance of $\psi(4040)$ is 8.0σ and those for $\psi(4230)$ and $\psi(4360)$ are more than 10.0σ .

DOI: [10.1103/PhysRevD.109.092012](https://doi.org/10.1103/PhysRevD.109.092012)

I. INTRODUCTION

Hadron spectroscopy is a fascinating field full of discoveries and surprises. Over the past decades, many charmonium-like states with $J^{PC} = 1^{--}$, called Y states, have been discovered and confirmed by numerous

experiments. As nonstandard hadron candidates beyond the conventional quark model, these states have many characteristics that are different from the traditional ones and have stimulated great interests both experimental and theoretical. The masses of these Y states are above $D\bar{D}$ threshold, and they have strong coupling to hidden-charm final states. Many theoretical interpretations, such as hybrid mesons, compact tetraquark states and hadronic molecules [1], have been proposed. However, none of them can account for all unusual properties of these Y states.

Among these exotic states, $\psi(4230)$, previously known as $Y(4260)$, and $\psi(4360)$, previously known as $Y(4360)$, were first discovered by *BABAR* and *Belle* using initial-state-radiation (ISR) in the $e^+e^- \rightarrow \gamma_{\text{ISR}}\pi^+\pi^-J/\psi$ [2–5] and $e^+e^- \rightarrow \gamma_{\text{ISR}}\pi^+\pi^-\psi(3686)$ [6–9] processes. With higher statistics achieved by BESIII, they are observed via more processes and measured with improved precision. The $\psi(4230)$ is observed in the $e^+e^- \rightarrow \pi^+\pi^-J/\psi$ [10,11], $e^+e^- \rightarrow \pi^0\pi^0J/\psi$ [12], $e^+e^- \rightarrow K_S^0K_S^0J/\psi$ [13], $e^+e^- \rightarrow K^+K^-J/\psi$ [14], $e^+e^- \rightarrow \pi^+\pi^-\psi(3686)$ [15,16], $e^+e^- \rightarrow \pi^+\pi^-h_c$ [17], $e^+e^- \rightarrow \omega\chi_{c0}$ [18,19], and $e^+e^- \rightarrow \pi^+D^0D^{*-}$ [20] processes, and the $\psi(4360)$ is observed in the $e^+e^- \rightarrow \pi^+\pi^-\psi(3686)$ [15,16], $e^+e^- \rightarrow \pi^+\pi^-h_c$ [17], and $e^+e^- \rightarrow \pi^+\pi^-\psi_2(3823)$ [21] processes. The parameters of each of these two resonances, such as their masses and widths, are similar, but there are still differences between these decay modes.

In recent years, the branching fractions, partial decay widths, and the quark components of $\psi(4230)$ and $\psi(4360)$ have been predicted by many theoretical models. Assuming the $\psi(4230)$ is a conventional $\psi(4S)$ state and using the electronic partial widths provided by Refs. [22,23], the upper limit of the $\psi(4S) \rightarrow \eta J/\psi$ branching fraction is predicted to be 1.9×10^{-3} [24]. Assuming that $\psi(4360)$ is a pure $4(3^3D_1)$ state, the partial width of the $\psi(4360) \rightarrow \eta J/\psi$ decay is estimated in Ref. [25]. Assuming a hadronic

^aAlso at the Moscow Institute of Physics and Technology, Moscow 141700, Russia.

^bAlso at the Novosibirsk State University, Novosibirsk, 630090, Russia.

^cAlso at the NRC “Kurchatov Institute,” PNPI, 188300, Gatchina, Russia.

^dAlso at Goethe University Frankfurt, 60323 Frankfurt am Main, Germany.

^eAlso at Key Laboratory for Particle Physics, Astrophysics and Cosmology, Ministry of Education; Shanghai Key Laboratory for Particle Physics and Cosmology; Institute of Nuclear and Particle Physics, Shanghai 200240, People's Republic of China.

^fAlso at Key Laboratory of Nuclear Physics and Ion-beam Application (MOE) and Institute of Modern Physics, Fudan University, Shanghai 200443, People's Republic of China.

^gAlso at State Key Laboratory of Nuclear Physics and Technology, Peking University, Beijing 100871, People's Republic of China.

^hAlso at School of Physics and Electronics, Hunan University, Changsha 410082, China.

ⁱAlso at Guangdong Provincial Key Laboratory of Nuclear Science, Institute of Quantum Matter, South China Normal University, Guangzhou 510006, China.

^jAlso at MOE Frontiers Science Center for Rare Isotopes, Lanzhou University, Lanzhou 730000, People's Republic of China.

^kAlso at Lanzhou Center for Theoretical Physics, Lanzhou University, Lanzhou 730000, People's Republic of China.

^lAlso at the Department of Mathematical Sciences, IBA, Karachi 75270, Pakistan.

molecular state, Refs. [26,27] predict the partial decay widths or branching fractions of $\eta J/\psi$ and other final states for $\psi(4230)$ and $\psi(4360)$ decays.

In this paper, an updated analysis of $e^+e^- \rightarrow \eta J/\psi$ at 44 center-of-mass (c.m.) energies between 3.808 and 4.951 GeV is performed, using a similar approach as in Ref. [28]. Additional data samples on the side of the $\psi(4230)$ peak and from 4.612 to 4.951 GeV are used, which can describe $\psi(4230)$, $\psi(4360)$ and the nonresonance more precisely than the previous measurement [28], as well as allow a search for heavier Y states in the $e^+e^- \rightarrow \eta J/\psi$ process. In this analysis, the J/ψ is reconstructed via $J/\psi \rightarrow \ell^+\ell^-$ ($\ell = e/\mu$), and the η is reconstructed via $\eta \rightarrow \gamma\gamma$ (Mode I) and $\eta \rightarrow \pi^0\pi^+\pi^-$ (Mode II).

II. THE BESIII DETECTOR AND DATA SAMPLES

The BESIII detector [29] records symmetric e^+e^- collisions provided by the BEPCII storage ring [30]. The cylindrical core of the BESIII detector covers 93% of the full solid angle and consists of a helium-based multilayer drift chamber (MDC), a plastic scintillator time-of-flight system (TOF), and a CsI(Tl) electromagnetic calorimeter (EMC), which are all enclosed in a superconducting solenoidal magnet providing a 1.0 T magnetic field. The solenoid is supported by an octagonal flux-return yoke with resistive plate counter muon identification modules interleaved with steel. The charged-particle momentum resolution at 1 GeV/ c is 0.5%, and the specific ionization energy loss dE/dx resolution is 6% for electrons from Bhabha scattering. The EMC measures photon energies with a resolution of 2.5% (5%) at 1 GeV in the barrel (end cap) region. The time resolution in the TOF barrel region is 68 ps, while that in the end cap region was 110 ps. The end cap TOF system was upgraded in 2015 using multigap resistive plate chamber technology, providing a time resolution of 60 ps [31].

The data samples used in this analysis are listed in Appendix A. Among them, 76.05% are collected after the end cap TOF upgrade. The c.m. energy is measured using dimuon events with a precision of 0.8 MeV for data samples with \sqrt{s} lower than 4.612 GeV [32,33] and using $\Lambda_c^+\bar{\Lambda}_c^-$ events with a precision of 0.6 MeV for data samples with \sqrt{s} higher than or equal to 4.612 GeV [34]. The integrated luminosity is determined with an uncertainty of 1.0% by analyzing large-angle Bhabha scattering events [34–36].

Monte Carlo (MC) simulation is used to optimize event selection criteria, estimate background, and determine event selection efficiencies. The BESIII MC simulation framework is based on GEANT4 [37] and includes the geometric description [38] of the BESIII detector and the realistic representation of the electronic readout. The beam energy spread and ISR in the e^+e^- annihilation are modeled with the KKMC generator [39,40]. The inclusive MC sample includes the production of open charm processes, the ISR

production of vector charmonium(-like) states, and the nonresonant processes incorporated in KKMC. All particle decays are modeled with EVTGEN [41,42] using branching fractions either taken from the Particle Data Group (PDG) [43], when available, or otherwise estimated with LUNDCHARM [44,45], CONEXC [46] and PHOKHARA [47]. Final state radiation from charged final state particles is incorporated using PHOTOS [48]. Signal MC samples of $e^+e^- \rightarrow \eta J/\psi$ with the corresponding J/ψ and η decay modes are generated using HELAMP [41] with parameters (1 0 0 0 -1 0) and EVTGEN at each c.m. energy. ISR is simulated with KKMC, and the maximum energy of the ISR photon is adjusted according to the $\eta J/\psi$ mass threshold.

III. EVENT SELECTION

The good charged tracks are required to be within the angle coverage of the MDC, $|\cos\theta| < 0.93$, where the θ is defined with respect to the z axis, which is the symmetry axis of the MDC. The distance of closest approach to the e^+e^- interaction point must be less than 1 cm in the transverse plane, $|V_{xy}| < 1$ cm, and less than 10 cm along the z axis, $|V_z| < 10$ cm. Photon candidates are identified using showers in the EMC. The deposited energy of each shower must be more than 25 MeV in the barrel region ($|\cos\theta| < 0.80$) and more than 50 MeV in the end cap region ($0.86 < |\cos\theta| < 0.92$). To suppress electronic noise and showers unrelated to the event, the difference between the EMC time and the event start time is required to be within [0, 700] ns. To remove photons produced by interactions of charged tracks, the opening angle between a shower and its nearest charged track has to be greater than 20° . Candidate events are required to have two (Mode I) or four (Mode II) charged tracks with zero net charge and at least two photons.

For signal candidates, the pions and leptons are distinguished by their momenta. The charged tracks with momenta above 1.0 GeV/ c are assigned to be leptons, while others are assumed to be pions. The separation of electrons and muons is accomplished using the deposited energy (E) in the EMC. Muons must satisfy $E \leq 0.4$ GeV, while electrons must satisfy $E/p > 0.8$, where p is the momentum of the charged track. For Mode I, signal candidate events are required to have a lepton pair with the same flavor and opposite charge, and at least two photons. For Mode II, two additional pions with opposite charge are required.

To improve the resolution and suppress the background for Mode I, a four-constraint (4C) kinematic fit imposing energy-momentum conservation is performed under the hypothesis $e^+e^- \rightarrow \gamma\gamma\ell^+\ell^-$. For Mode II, a five-constraint (5C) kinematic fit is performed under the hypothesis $e^+e^- \rightarrow \gamma\gamma\pi^+\pi^-\ell^+\ell^-$ with an additional π^0 mass constraint for the photon pair. For candidate events with more than two photons, the combination with the smallest χ^2_{4C} or

χ^2_{5C} of the 4C or 5C kinematic fit is retained. We require $\chi^2_{4C} < 40$ for Mode I and $\chi^2_{5C} < 80$ for Mode II. For Mode I, to suppress the background from radiative Bhabha and dimuon processes, the energy of each selected photon after the 4C kinematic fit is required to be greater than 0.08 GeV.

Figure 1 shows the distributions of the invariant mass of the $\ell^+\ell^-$ pair ($M(\ell^+\ell^-)$) versus those of the $\gamma\gamma$ pair ($M(\gamma\gamma)$) or $\pi^0\pi^+\pi^-$ ($M(\pi^0\pi^+\pi^-)$) for selected events of the data sample at $\sqrt{s} = 4.226$ GeV. A clear enhancement from the signal events appears at the intersection of the J/ψ and η mass regions in data. Because of the much larger cross section of the radiative Bhabha process, the background in $J/\psi \rightarrow e^+e^-$ is more serious than for $J/\psi \rightarrow \mu^+\mu^-$ in Mode I. Signal candidates are required to be within the J/ψ mass region, defined as [3.067, 3.127] GeV/ c^2 on $M(\ell^+\ell^-)$. The events in the J/ψ mass sideband regions, defined as [3.027, 3.057] and [3.137, 3.167] GeV/ c^2 , are

used to estimate the non- J/ψ background, and no peaking background is observed in the $M(\gamma\gamma)$ or $M(\pi^0\pi^+\pi^-)$ distributions.

IV. CROSS SECTION MEASUREMENT

The Born cross section σ^B is determined by

$$\sigma^B = \frac{N_{\text{sig}}}{\mathcal{L}_{\text{int}} \cdot (1 + \delta^{\text{ISR}}) \cdot \frac{1}{|1-\Pi|^2} \cdot \mathcal{B} \cdot \epsilon}, \quad (1)$$

where N_{sig} is the signal yield observed from the fit of the mass spectrum, as shown in Fig. 1, \mathcal{L}_{int} is the integrated luminosity, $(1 + \delta^{\text{ISR}})$ is the ISR correction factor, $\frac{1}{|1-\Pi|^2}$ is the vacuum polarization factor taken from Ref. [49], \mathcal{B} is the product of the branching fractions of the intermediate states in the subsequent decays from the PDG [43], and ϵ is the signal detection efficiency. The ISR correction factor and the detection efficiency are estimated based on signal MC samples, and weighted by a dressed cross section iterative weighting method [50]. The relationship between the dressed cross sections and the Born cross sections is described by $\sigma^{\text{dressed}} = \frac{\sigma^B}{|1-\Pi|^2}$.

The measured cross section for each c.m. energy is directly obtained by a simultaneous unbinned maximum-likelihood fit to the $M(\gamma\gamma)$ and $M(\pi^0\pi^+\pi^-)$ spectra extracted from the $J/\psi \rightarrow e^+e^-$ and $J/\psi \rightarrow \mu^+\mu^-$ modes separately, where the cross section is considered as a shared parameter between the four studied final states by Eq. (1). The signal shape is described by a simulated shape convolved with a Gaussian function, which accounts for the difference of resolution between data and MC simulation. Among different data samples, the parameters of this Gaussian function are common and fixed to two different sets of values for Mode I and Mode II. To determine the parameters, simultaneous fits to the $M(\gamma\gamma)$ and $M(\pi^0\pi^+\pi^-)$ are performed, using data samples with large statistics ($\sqrt{s} = 4.178, 4.209, 4.219, 4.226, 4.258$ and 4.416 GeV). The background shape is described by a linear function.

Our measurements are in good agreement with earlier results from BESIII [28,51,52] and with Belle [53]. The measured cross sections and comparison between different experiments are shown in Fig. 2. The small differences between this analysis and the previous BESIII results are due to increased statistics of data samples with the same c.m. energy and the updated parameters of the HELAMP generator. The cross sections and quantities used for their measurements are summarized in Appendix A.

For those collision energy points where the statistics are insufficient to observe a signal significance above 5σ , upper limits are also estimated. The obtained normalized likelihood distribution as a function of the cross section, denoted as $F_j(\sigma^{\text{dressed}})$ for the j th energy point, is parametrized by a sum of two Gaussian functions with floated

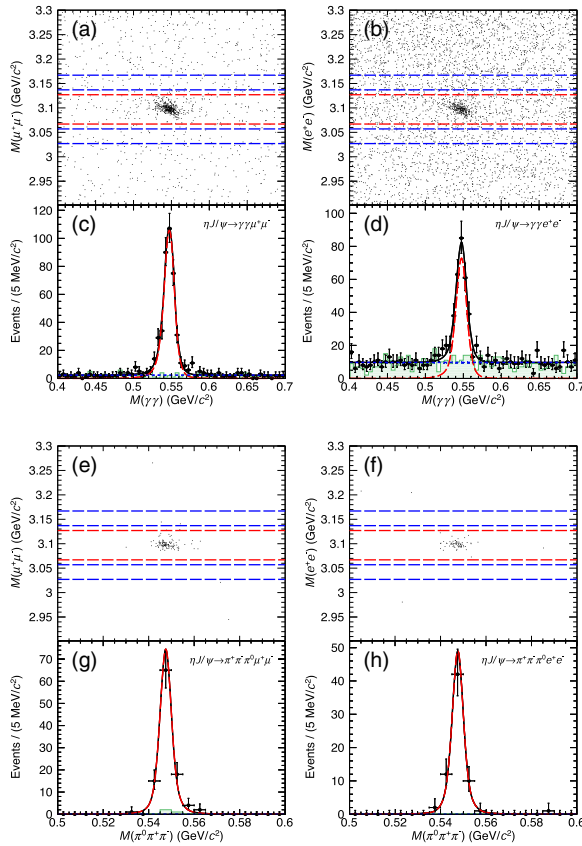


FIG. 1. (a), (b), (e), and (f) are the distributions of $M(\ell^+\ell^-)$ versus $M(\gamma\gamma/\pi^0\pi^+\pi^-)$, where the region enclosed by red (blue) long-dashed lines is the signal (sideband) region. (c), (d), (g), and (h) are the distributions of $M(\gamma\gamma/\pi^0\pi^+\pi^-)$ in the J/ψ signal region of the data sample at $\sqrt{s} = 4.226$ GeV, where the dots with error bars show data, the green histogram shows the events from the J/ψ mass sideband, the black solid, red long-dashed and blue short-dashed lines denote the fit result, signal, and background, respectively. The top (bottom) four panels correspond to Mode I (Mode II).

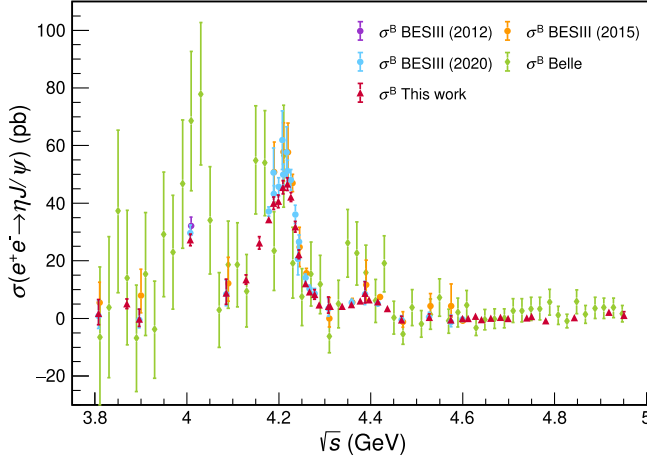


FIG. 2. The Born cross sections of $e^+e^- \rightarrow \eta J/\psi$. The purple, orange and pale blue dots with error bars are the Born cross sections measured previously at BESIII [28,51,52]; the green diamonds with error bars are the Belle results [53]; and the red triangles with error bars are the nominal Born cross sections from this work. The errors shown are the quadratic sum of statistical and systematic uncertainties.

mean, width and coefficient, respectively. And it will be used in the subsequent cross section line shape fit mentioned in Sec. V. The red line shown in Fig. 3 is the likelihood distribution at $\sqrt{s} = 3.896$ GeV as an example. Thus, with a uniform prior probability density function, the Bayesian upper limit for the cross section at 90% confidence level (CL) is estimated by integrating the likelihood distribution $F_i(\sigma^{\text{dressed}})$ from zero to the value that gives 90% of the total area as in Ref. [54]. Before integrating, the systematic uncertainties are taken into account as in Refs. [55–57].

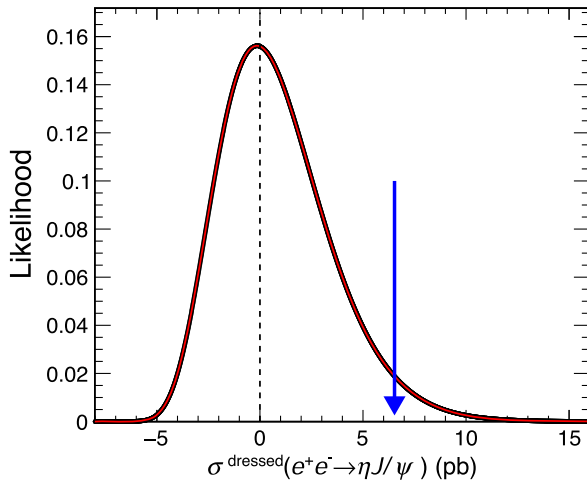


FIG. 3. The likelihood distribution as a function of the dressed cross section at $\sqrt{s} = 3.896$ GeV. The blue arrow refers to the 90% C.L. upper limit on the cross section.

V. FIT TO THE CROSS SECTION

According to the three evident peaks in the dressed cross section spectrum, a simplified fit model is parametrized as a coherent sum of three Breit-Wigner functions, describing the structures around 4040, 4220 and 4390 MeV/ c^2 , and a nonresonant component:

$$\sigma^{\text{fit}}(\sqrt{s}) = \left| \sqrt{\sigma_{NY}(\sqrt{s})} + \sum_{j=1}^3 BW_j(\sqrt{s}) e^{i\phi_j} \right|^2, \quad (2)$$

where the i is the imaginary unit, the ϕ_j is the relative phases between three resonances and the nonresonant. Under this physical assumption, the value of the cross section $\sigma^{\text{fit}}(\sqrt{s})$ should be non-negative.

The resonance is parametrized as the Breit-Wigner function BW_j with the two-body phase space factor $\Phi(\sqrt{s})$:

$$BW_j(\sqrt{s}) = \frac{\sqrt{12\pi\mathcal{B}_j\Gamma_j^{e^+e^-}\Gamma_j}}{s - M_j^2 + iM_j\Gamma_j} \sqrt{\frac{\Phi(\sqrt{s})}{\Phi(M_j)}}, \quad (3)$$

$$\Phi(\sqrt{s}) = \frac{q^3}{s}. \quad (4)$$

In Eq. (3), \mathcal{B}_j , $\Gamma_j^{e^+e^-}$, Γ_j and M_j denote the resonance decay branching fraction to the $\eta J/\psi$ final state, the partial width of its decay to e^+e^- , the full width, and the mass of the j th resonance. In Eq. (4), q is the daughter momentum in the rest frame of its parent.

The non-resonant part is parametrized following the method of BABAR [4] as

$$\sqrt{\sigma_{NY}(\sqrt{s})} = \sqrt{\Phi(\sqrt{s})} e^{-p_0 u} p_1, \quad (5)$$

where p_0 and p_1 are free parameters, and $u = \sqrt{s} - (M_\eta + M_{J/\psi})$.

To study these possible resonances in the $e^+e^- \rightarrow \eta J/\psi$ process, a maximum-likelihood fit is performed to the dressed cross sections. For each data sample with large statistics, the likelihood that represents the deviation between the fit cross section and the measured one is evaluated by a normalized Gaussian distribution as

$$G_i(\sigma_i^{\text{fit}}; \sigma_i, \theta_i) = \frac{1}{\theta_i \sqrt{2\pi}} e^{-\frac{(\sigma_i^{\text{fit}} - \sigma_i)^2}{2\theta_i^2}}, \quad (6)$$

where the mean σ_i and the width θ_i is the measured cross section and the corresponding statistical uncertainties of the i th energy point. In cases where the data sample lacks a significant signal, the likelihood shape $F_j(\sigma_j^{\text{fit}})$ obtained from the process of upper limit estimation is used to

TABLE I. Results of the fits to the $e^+e^- \rightarrow \eta J/\psi$ cross sections. M_i , Γ_i , $\Gamma_i^{e^+e^-}$, \mathcal{B}_i and ϕ_i represent the parameters shown in Eq. (2), Eq. (3) and Eq. (5). The label $i = 1, 2$ and 3 symbolizes $\psi(4040)$, $\psi(4230)$, and $\psi(4360)$, respectively. The uncertainties are statistical only.

Parameter	Solution I	Solution II	Solution III	Solution IV
M_1 (MeV/ c^2)		4039 (fixed)		
Γ_1 (MeV)		80 (fixed)		
$\Gamma_1^{e^+e^-} \cdot \mathcal{B}_1$ (eV)	1.0 ± 0.2	7.1 ± 0.6	1.1 ± 0.2	7.8 ± 0.6
M_2 (MeV/ c^2)		4219.7 ± 2.5		
Γ_2 (MeV)		80.7 ± 4.4		
$\Gamma_2^{e^+e^-} \cdot \mathcal{B}_2$ (eV)	4.0 ± 0.5	5.5 ± 0.7	8.7 ± 1.0	11.9 ± 1.1
M_3 (MeV/ c^2)		4386.4 ± 12.6		
Γ_3 (MeV)		176.9 ± 32.1		
$\Gamma_3^{e^+e^-} \cdot \mathcal{B}_3$ (eV)	1.8 ± 0.6	2.1 ± 0.7	4.3 ± 1.3	5.0 ± 1.5
ϕ_1 (rad)	3.1 ± 0.6	-1.8 ± 0.1	3.3 ± 0.4	-1.6 ± 0.1
ϕ_2 (rad)	-2.8 ± 0.1	2.9 ± 0.2	-2.0 ± 0.1	-2.6 ± 0.2
ϕ_3 (rad)	-2.9 ± 0.1	3.0 ± 0.1	2.8 ± 0.1	2.4 ± 0.7
p_0 (MeV $^{-1}$)	1.5 ± 0.4	1.5 ± 0.4	1.5 ± 0.4	1.6 ± 0.4
p_1 (GeV $^{-3}$)	390.0 ± 155.3	389.3 ± 155.6	389.5 ± 155.1	389.5 ± 154.5

describe the cross section at the j th energy point, as mentioned before.

Therefore, the likelihood function of all data samples is composed of two parts as

$$L = \prod_{i=1}^{N_1=22} G_i(\sigma_i^{\text{fit}}) \cdot \prod_{j=1}^{N_2=22} F_j(\sigma_j^{\text{fit}}), \quad (7)$$

where the N_1 denotes the number of the data samples with large statistics, and the N_2 denotes those lacking a significant signal.

In this fit, the structure around 4040 MeV/ c^2 is assumed to be $\psi(4040)$. Because of the lack of data samples around this energy region, the mass and width of the $\psi(4040)$ are fixed to the values given in the PDG [43]. By scanning three relative phases, four solutions with similar fit quality and identical masses and widths of the resonances around 4220 and 4390 MeV/ c^2 are found, consistent with the mathematical analysis of multiple solutions shown in Ref. [58]. The fit quality is $\chi^2/\text{d.o.f.} = 66.9/44$, estimated by a χ^2 -test approach, where d.o.f. is the number of degrees of freedom. The fit results are shown in Table I and Fig. 4. To estimate the significance of the three structures and the nonresonant part, the fits are repeated removing one of these four terms at a time. The statistical significances of both the nonresonant part and $\psi(4040)$ are 8.0σ , and those of the $\psi(4230)$ and $\psi(4360)$ are more than 10.0σ .

Alternative fits are carried out by replacing the second resonance with $\psi(4160)$ parameters and the third resonance with $\psi(4360)$ or $\psi(4415)$ parameters from the PDG [43]. However, their fit qualities are significantly worse than the nominal results and cannot describe the data well. To search for the existence of other potential resonances, fits are performed by adding the $\psi(4160)$ or $\psi(4415)$ component

with the fixed parameters from the PDG [43]. The significances of $\psi(4160)$ and $\psi(4415)$ are 3.2σ and 1.1σ , respectively. A fit is also performed with an additional Breit-Wigner function with free parameters, whose significance is 3.3σ . In this case, the significances of previous three resonances have not decreased, and those of $\psi(4230)$ and $\psi(4360)$ are still much greater than 10.0σ . The mass and width of this extra resonance are (4151 ± 20) MeV/ c^2 and (110 ± 36) MeV, and the parameters of $\psi(4230)$ and $\psi(4360)$ turn out to be (4226.5 ± 3.3) MeV/ c^2 and (56.8 ± 7.4) MeV, and (4412.0 ± 6.9) MeV/ c^2 and (82 ± 20) MeV, respectively.

VI. SYSTEMATIC UNCERTAINTY

A. Systematic uncertainties for cross section measurement

The following sources of systematic uncertainties are considered in the cross section measurement listed in Appendix B. The uncertainty of the integrated luminosity is estimated to be 1.0% using large-angle Bhabha scattering events [34–36]. The uncertainty of the charged track reconstruction efficiency is estimated to be 1.0% for each lepton [59]. The charged pion is only reconstructed in Mode II. The uncertainty from the pion pair reconstruction efficiency for Mode II is 2.0%, [60]. The uncertainty of the reconstruction efficiency per photon is estimated to be 1.0% [61]. The uncertainties of the branching fractions of the intermediate decays are taken from the PDG [43]. The uncertainty of the radiative correction includes two parts. The first part stems from the precision of the ISR calculation in the generator κMC . The other part stems from $(1 + \delta^{\text{ISR}})$ and ϵ in Eq. (1), and depends on the input line shape of the cross section. Therefore, in order to estimate the uncertainty related to ISR correction,

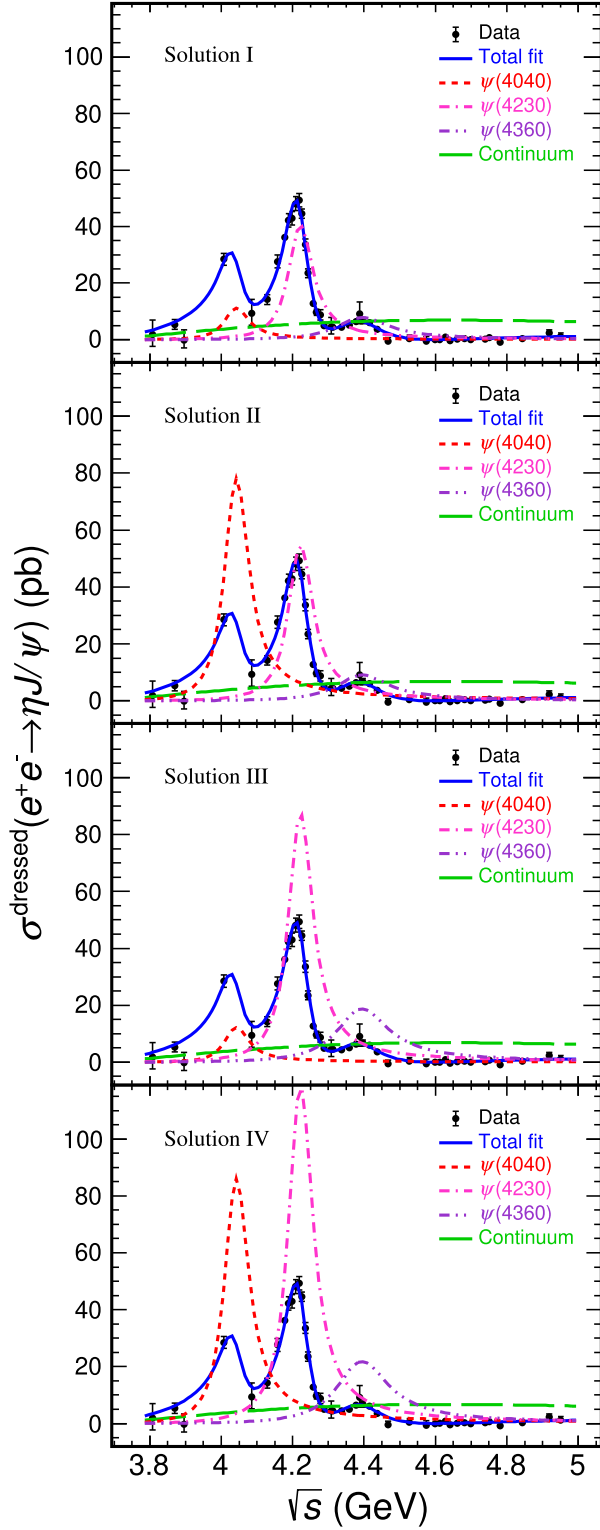


FIG. 4. The fits to the dressed cross sections of $e^+e^- \rightarrow \eta J/\psi$ corresponding to the four solutions in Table I. The black dots with error bars are the measured dressed cross sections, and the blue solid curves represent the best fit results of the following interfering amplitudes: $\psi(4040)$ (dashed red), $\psi(4230)$ (short-dashed pink), $\psi(4360)$ (short-dashed purple), and the nonresonant component (long-dashed green).

$(1 + \delta^{\text{ISR}}) \cdot \epsilon$ is evaluated 500 times by varying the input cross section line shape parameters with the uncertainties and the covariance matrix obtained from the nominal result. The standard deviation of the $(1 + \delta^{\text{ISR}}) \cdot \epsilon$ distribution is considered as the systematic uncertainty. The uncertainty associated with the J/ψ mass requirement is estimated by smearing the $M(\ell^+\ell^-)$ distribution of MC samples according to the resolution difference between data and MC simulation, and the resulting uncertainties in signal efficiencies are obtained. For the uncertainty from the kinematic fit, we correct the helix parameters of the charged tracks in the MC to match the pull distributions in the data [62] and reevaluate the selection efficiencies. The resulting changes of cross sections are considered as the systematic uncertainties. The systematic uncertainty of the photon-energy criteria in Mode I is considered by the “Barlow-test,” following the procedure described in Refs. [63,64]. The uncertainties related to the fit procedure are estimated by changing the fit range, replacing the first-order polynomial function by a second-order polynomial function for the background description, and varying the width of the convolved Gaussian function for the signal shape by 1 standard deviation. The uncertainties from the other selections, trigger simulation, event start time determination, and final-state-radiation simulation and other sources, are conservatively taken as 1.0%. Assuming all sources of systematic uncertainties to be independent, the total uncertainties in the $e^+e^- \rightarrow \eta J/\psi$ cross sections are assigned as the quadratic sum of the individual items, which are 3.8% ~ 27.9% and shown in Appendix C.

B. Systematic uncertainties for resonance parameters

The systematic uncertainties for the resonance parameters in the cross section fit are as follows. The systematic uncertainty associated with the collision energy is conservatively estimated to be 0.8 MeV [32,33]. It is common for all data samples and causes a global uncertainty of the mass measurement of Y states. The uncertainty due to the energy spread is estimated by convolving the fit formula with a Gaussian function with a width of 1.6 MeV, which is the energy spread determined by the beam energy measurement system [65]. The uncertainties associated with the cross section measurement are estimated by incorporating the correlated and uncorrelated systematic uncertainties of the measured cross sections in the fit as shown in Appendix C. The uncertainties from the $\psi(4040)$ resonance parameters are studied by varying the parameters within their uncertainties from the PDG [43]. To estimate the uncertainty related to the parametrization of the nonresonant part, we replace its amplitude in Eq. (5) with $\frac{C_0}{s^h} \sqrt{\Phi(\sqrt{s})}$, where C_0 is a free parameter and $\Phi(\sqrt{s})$ is defined in Eq. (4). To estimate the uncertainty from the parametrization of the Breit-Wigner function, Γ_i is set to the mass dependent width $\Gamma_i = \Gamma_i^0 \cdot \frac{\Phi(\sqrt{s})}{\Phi(M_i)}$, where Γ_i^0 is the

TABLE II. Systematic uncertainties of resonance parameters, including the c.m. energy (\sqrt{s}), the energy spread (\sqrt{s} spread), the $\psi(4040)$ parameters ($\psi(4040)$), the systematic uncertainty in the cross section measurement (Cross section), the parametrization of nonresonant amplitude (Fit model), and the parametrization of the Breit-Wigner function (Γ_{tot}). The symbol “...” represents that the uncertainty is neglected. The label $i = 1, 2$ and 3 symbolizes $\psi(4040)$, $\psi(4230)$, and $\psi(4360)$, respectively.

Source	Solution	\sqrt{s}	\sqrt{s} spread	$\psi(4040)$	Cross section	Fit model	Γ_{tot}	Total
M_2 (MeV/ c^2)	–	0.8	0.7	0.3	0.7	0.2	4.3	4.5
Γ_2 (MeV)	–	...	1.1	0.3	0.9	0.2	0.3	1.4
M_3 (MeV/ c^2)	–	0.8	0.4	1.1	0.8	0.1	16.8	16.9
Γ_3 (MeV)	–	...	9.9	0.8	6.7	4.7	2.0	13.0
$\Gamma_1^{e^+e^-} \cdot \mathcal{B}_1$ (eV)	I	...	0.05	0.09	0.04	0.01	0.05	0.12
	II	...	0.03	0.87	0.04	0.01	0.31	0.93
	III	...	0.05	0.11	0.05	0.01	0.06	0.15
	IV	...	0.04	1.06	0.03	0.01	0.38	1.13
$\Gamma_2^{e^+e^-} \cdot \mathcal{B}_2$ (eV)	I	...	0.02	0.03	0.10	0.02	0.01	0.11
	II	...	0.12	0.26	0.06	0.00	0.10	0.31
	III	...	0.18	0.05	0.34	0.12	0.03	0.41
	IV	...	0.05	0.40	0.30	0.10	0.23	0.57
$\Gamma_3^{e^+e^-} \cdot \mathcal{B}_3$ (eV)	I	...	0.18	0.00	0.16	0.09	0.01	0.26
	II	...	0.22	0.04	0.18	0.10	0.02	0.30
	III	...	0.30	0.05	0.30	0.16	0.01	0.45
	IV	...	0.36	0.14	0.34	0.17	0.03	0.54

nominal width of the resonance. We perform the fit to the cross section line shape with the above scenarios individually, and the resultant differences are taken as the systematic uncertainties, listed in Table II. The total systematic uncertainty is obtained by summing all sources of systematic uncertainties in quadrature, under the assumption that they are uncorrelated.

VII. SUMMARY AND DISCUSSION

In summary, we measure the cross sections of $e^+e^- \rightarrow \eta J/\psi$ at c.m. energies between 3.808 and 4.951 GeV using data samples with an integrated luminosity of 22.42 fb $^{-1}$ collected by the BESIII detector operating at the BEPCII collider. The measured Born cross sections are consistent with the previous BESIII measurements [28,51,52]. However, additional cross sections are measured on both sides of the $\psi(4230)$ peak, and from 4.612 to 4.951 GeV, allowing the line shape to be studied more precisely than before.

The dressed cross sections are fitted with a simplified model based on the evident peaks in the cross section spectrum, which includes three resonances and a nonresonant component. Assuming the lowest lying structure as $\psi(4040)$, the $\psi(4230)$ and $\psi(4360)$ structures are clearly observed with statistical significance much greater than 10.0σ . The masses and widths of these two states are determined as $M = (4219.7 \pm 2.5 \pm 4.5)$ MeV/ c^2 , $\Gamma = (80.7 \pm 4.4 \pm 1.4)$ MeV for $\psi(4230)$, and $M = (4386 \pm 13 \pm 17)$ MeV/ c^2 , $\Gamma = (177 \pm 32 \pm 13)$ MeV for $\psi(4360)$, respectively. A comparison of the parameters of $\psi(4230)$ and $\psi(4360)$ obtained in this analysis and the previous

BESIII ones is shown in Fig. 5. The parameters of $\psi(4360)$ are consistent within uncertainties. However, the width of $\psi(4230)$ obtained in this analysis is larger than those obtained in other processes [11,12,16,19].

Based on the four solutions including the statistical and systematic uncertainties and combining with the electronic partial widths, which are 0.63–0.66 keV for $\psi(4230)$ and 0.523 keV for $\psi(4360)$ in Refs. [24,25], the branching fraction $\mathcal{B}(\psi(4230) \rightarrow \eta J/\psi)$ is estimated to be in the range of $(6.06 \pm 0.76 \pm 0.17) \times 10^{-3}$ to $(18.89 \pm 1.75 \pm 0.90) \times 10^{-3}$, and the partial decay width

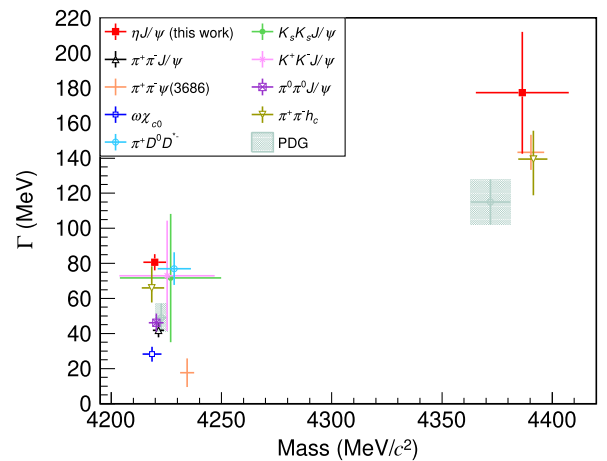


FIG. 5. Comparison of masses versus widths of $\psi(4230)$ and $\psi(4360)$ from the previous BESIII measurements [11–14,16,17,19,20] and the average values in the PDG [43]. The results in the bottom left are for $\psi(4230)$, and the ones in the top right are for $\psi(4360)$.

$\Gamma(\psi(4360) \rightarrow \eta J/\psi)$ is estimated to be in the range of $(0.61 \pm 0.23 \pm 0.10)$ MeV to $(1.70 \pm 0.59 \pm 0.22)$ MeV. But neither of them can cover the predictions of Refs. [24,25] based on a conventional charmonium state model. Comparing with $\Gamma_{\psi(4360)}^{e^+e^-} \cdot \mathcal{B}(\psi(4360) \rightarrow \pi^+\pi^-h_c)$ from Ref. [17], we obtain the ratio $\frac{\Gamma(\psi(4360) \rightarrow \eta J/\psi)}{\Gamma(\psi(4360) \rightarrow \pi^+\pi^-h_c)} = 0.16_{-0.07}^{+0.08} \pm 0.03 \sim 0.43_{-0.21}^{+0.23} \pm 0.08$, which is beyond the expected range under the $D^*\bar{D}_1 + \text{H.c.}$ ¹ molecular scenario in Ref. [27]. Further theoretical and experimental studies are still needed to interpret the nature and the structures of these states.

ACKNOWLEDGMENTS

The BESIII Collaboration thanks the staff of BEPCII and the IHEP computing center and the supercomputing center of the University of Science and Technology of China (USTC) for their strong support. This work is supported in part by National Key R&D Program of China under Contracts No. 2020YFA0406400 and No. 2020YFA0406300; National Natural Science Foundation of China (NSFC) under Contracts No. 11335008, No. 11625523, No. 12035013, No. 11705192, No. 11950410506, No. 12061131003, No. 12105276, No. 12122509, No. 11635010, No. 11735014, No. 11835012, No. 11935015, No. 11935016, No. 11935018, No. 11961141012, No. 12022510, No. 12025502, No. 12035009, No. 12192260, No. 12192261, No. 12192262, No. 12192263, No. 12192264, No. 12192265, No. 12221005, No. 12225509, No. 12235017, and No. 12005311; the Chinese Academy of Sciences (CAS) Large-Scale Scientific Facility Program; the CAS Center for Excellence in Particle Physics (CCEPP); Joint Large-Scale Scientific Facility Funds of the NSFC and CAS under Contracts No. U1732263, No. U1832103, No. U2032111, and No. U1832207; CAS Key Research Program of Frontier Sciences under Contracts No. QYZDJ-SSW-SLH003 and No. QYZDJ-SSW-SLH040; 100 Talents Program of CAS; The Institute of Nuclear and Particle Physics (INPAC) and Shanghai Key Laboratory for Particle Physics and Cosmology; European Union’s Horizon 2020 research and innovation program under Marie Skłodowska-Curie Grant Agreement under Contract No. 894790; German Research Foundation DFG under Contract No. 455635585, Collaborative Research Center CRC 1044, FOR5327, GRK 2149; Istituto Nazionale di Fisica Nucleare, Italy; Ministry of Development of Turkey under Contract No. DPT2006K-120470; National Research Foundation of Korea under Contract No. NRF-2022R1A2C1092335; National Science and Technology fund of Mongolia; National Science Research and

Innovation Fund (NSRF) via the Program Management Unit for Human Resources & Institutional Development, Research and Innovation of Thailand under Contract No. B16F640076; Polish National Science Centre under Contract No. 2019/35/O/ST2/02907; The Swedish Research Council; and the U.S. Department of Energy under Contract No. DE-FG02-05ER41374.

APPENDIX A: SUMMARY OF THE BORN CROSS SECTIONS

Table III shows the values relating to the details of the calculation of the Born section. σ^{UL} denotes an estimate of the upper limit of the cross section at the 90% confidence level.

APPENDIX B: SYSTEMATIC UNCERTAINTIES ON THE CROSS SECTIONS

All systematic uncertainties at individual c.m. energies are summarized in Table IV. The sources with the symbol “*” are the correlated systematic uncertainties for different data samples. Due to the limited statistics of most data samples, the items with the symbol “†”, are estimated with the data sample with the highest statistics ($\sqrt{s} = 4.226$ GeV). The total systematic uncertainties are obtained with the quadrature sum of individual uncertainties by assuming all of them are independent.

APPENDIX C: DEFINITION OF LIKELIHOOD FUNCTION CONSIDERING THE SYSTEMATIC UNCERTAINTIES OF CROSS SECTIONS

In the maximum-likelihood fit of the dressed cross sections of $e^+e^- \rightarrow \eta J/\psi$, to consider the systematic uncertainties of resonance parameters from the cross section measurement, the systematic uncertainties of cross section measurement are divided into two parts, uncorrelated and correlated. Assuming all sources to be independent, the total uncorrelated and correlated relative systematic uncertainties are obtained by adding their individual values in quadrature separately.

(1) Uncorrelated part

The likelihood function of the i th data sample, considering the uncorrelated uncertainty from cross section measurement as the nuisance parameter following the Gaussian distribution, is defined as

$$L'_i = \int L_i(\sigma_i^{\text{fit}} \cdot \epsilon) \times \text{Gauss}(\epsilon; 1, \epsilon_i^{\text{uncorr}}) d\epsilon, \quad (\text{C1})$$

where L_i is the likelihood function with only statistical uncertainties, σ_i^{fit} is the expected value of cross section and $\epsilon_i^{\text{uncorr}}$ is the total uncorrelated systematic uncertainty in the cross section measurement of the i th data sample.

¹Hermitian conjugate.

TABLE III. The c.m. energy, the corresponding luminosity \mathcal{L} , the detection efficiency ϵ^i , the ISR correction factor $1 + \delta^{\text{ISR}}$, vacuum polarization factor $\frac{1}{1-\Pi^{\text{ISR}}}$, the signal yield N_{sig} for different decay modes, and the obtained Born cross section at each energy point, where the first uncertainties for cross sections are statistical and the second systematic.

\sqrt{s} (GeV)	\mathcal{L} (pb $^{-1}$)	$\epsilon(\%)^a$	$\epsilon(\%)^b$	$\epsilon(\%)^c$	$\epsilon(\%)^d$	N_{sig}^a	N_{sig}^b	N_{sig}^c	N_{sig}^d	$1 + \delta^{\text{ISR}}$	$\frac{1}{1-\Pi^{\text{ISR}}}$	σ (pb)	σ^{UL} (pb)
3.8077	50.54	25.13	17.27	9.56	6.71	$0.52^{+1.45}_{-1.18}$	$0.76^{+2.11}_{-1.06}$	$0.12^{+0.32}_{-0.26}$	$0.17^{+0.46}_{-0.38}$	1.598	1.056	$1.51^{+4.18}_{-3.41} \pm 0.06$	8.71
3.8694	219.2	41.67	29.24	17.66	12.40	6.43 ± 2.15	9.16 ± 3.06	1.57 ± 0.52	2.23 ± 0.74	0.801	1.051	$5.07 \pm 1.69 \pm 0.20$	
3.8962	52.61	41.66	29.37	17.49	12.73	$-0.05^{+1.03}_{-0.79}$	$-0.07^{+1.46}_{-1.12}$	$-0.01^{+0.26}_{-0.20}$	$-0.02^{+0.35}_{-0.27}$	0.802	1.049	$-0.17^{+3.38}_{-2.50} \pm 0.01$	6.53
4.0076	482.0	42.21	29.96	17.96	13.08	76.49 ± 5.70	107.58 ± 8.02	19.19 ± 1.43	26.31 ± 1.96	0.791	1.044	$27.26 \pm 2.03 \pm 1.06$	
4.0855	52.86	35.51	25.12	15.02	10.64	$2.94^{+1.57}_{-1.31}$	$4.14^{+2.21}_{-1.85}$	$0.71^{+0.38}_{-0.32}$	$1.01^{+0.54}_{-0.45}$	1.007	1.051	$8.87^{+4.73}_{-3.97} \pm 0.36$	15.97
4.1285	401.5	36.87	26.20	15.21	11.10	31.44 ± 3.76	44.17 ± 5.29	7.66 ± 0.92	10.47 ± 1.25	0.896	1.052	$13.47 \pm 1.61 \pm 0.54$	
4.1574	408.7	39.35	27.80	16.20	11.73	61.44 ± 4.99	86.82 ± 7.05	14.89 ± 1.21	20.55 ± 1.67	0.831	1.053	$26.24 \pm 2.13 \pm 1.02$	
4.1784	3194.5	40.17	28.23	16.63	11.88	616.72 ± 15.56	876.10 ± 22.10	149.21 ± 3.76	208.48 ± 5.26	0.804	1.054	$34.29 \pm 0.87 \pm 1.30$	
4.1888	570.03	40.64	28.59	16.82	12.20	128.85 ± 7.05	182.85 ± 10.01	31.59 ± 1.73	43.49 ± 2.38	0.796	1.056	$39.97 \pm 2.19 \pm 1.52$	
4.1989	526.0	41.08	29.06	17.13	12.24	122.90 ± 6.69	173.44 ± 9.44	29.74 ± 1.62	41.58 ± 2.26	0.795	1.056	$40.66 \pm 2.21 \pm 1.55$	
4.2091	572.05	40.79	28.67	16.74	11.82	149.53 ± 7.48	212.38 ± 10.63	35.43 ± 1.77	50.11 ± 2.51	0.805	1.057	$45.54 \pm 2.28 \pm 1.73$	
4.2186	569.2	40.38	28.60	16.52	12.08	156.54 ± 7.44	220.64 ± 10.48	37.99 ± 1.80	51.88 ± 2.47	0.829	1.056	$46.67 \pm 2.22 \pm 1.82$	
4.2263	1100.9	40.43	28.44	16.55	12.12	283.09 ± 10.42	401.77 ± 14.79	69.32 ± 2.55	94.50 ± 3.48	0.863	1.056	$42.15 \pm 1.55 \pm 1.64$	
4.2357	530.3	39.07	27.41	15.83	11.42	106.46 ± 6.26	151.51 ± 8.91	25.51 ± 1.50	35.27 ± 2.07	0.927	1.056	$31.82 \pm 1.87 \pm 1.24$	
4.2436	593.98	37.54	26.26	15.06	10.78	86.28 ± 5.84	123.13 ± 8.33	20.35 ± 1.38	28.38 ± 1.92	1.001	1.056	$22.24 \pm 1.51 \pm 0.89$	
4.2580	828.4	33.28	23.16	13.36	9.63	68.93 ± 5.50	98.89 ± 7.89	16.48 ± 1.31	22.82 ± 1.82	1.198	1.054	$12.10 \pm 0.97 \pm 0.51$	
4.2668	531.1	30.00	20.93	11.80	8.37	34.38 ± 3.94	49.19 ± 5.64	7.90 ± 0.91	11.12 ± 1.27	1.358	1.053	$9.19 \pm 1.05 \pm 0.39$	
4.2777	175.7	25.80	18.11	9.92	7.11	10.42 ± 2.13	14.81 ± 3.03	2.35 ± 0.48	3.27 ± 0.67	1.585	1.053	$8.33 \pm 1.71 \pm 0.38$	
4.2879	502.4	22.89	15.90	8.56	6.21	16.43 ± 3.02	23.61 ± 4.35	3.69 ± 0.68	5.07 ± 0.93	1.774	1.053	$4.68 \pm 0.86 \pm 0.21$	
4.3079	45.08	20.15	14.04	7.71	5.59	$1.22^{+0.92}_{-0.69}$	$1.75^{+1.32}_{-0.99}$	$0.28^{+0.21}_{-0.16}$	$0.39^{+0.29}_{-0.22}$	1.835	1.052	$4.25^{+3.22}_{-2.41} \pm 0.19$	9.59
4.3121	501.2	20.17	14.33	7.65	5.54	13.44 ± 2.67	18.89 ± 3.75	2.99 ± 0.59	4.12 ± 0.82	1.787	1.052	$4.23 \pm 0.84 \pm 0.18$	
4.3374	505.0	23.19	16.59	9.02	6.49	$12.42^{+2.97}_{-2.74}$	$17.33^{+4.14}_{-3.82}$	$2.79^{+0.67}_{-0.62}$	$3.87^{+0.93}_{-0.85}$	1.430	1.051	$4.19^{+1.00}_{-0.92} \pm 0.17$	5.61
4.3583	543.9	26.53	18.63	10.41	7.47	15.05 ± 2.81	21.40 ± 4.00	3.47 ± 0.65	4.82 ± 0.90	1.241	1.051	$4.84 \pm 0.90 \pm 0.19$	
4.3774	522.7	28.58	19.75	10.83	7.92	18.21 ± 2.96	26.31 ± 4.28	4.20 ± 0.68	5.73 ± 0.93	1.171	1.051	$6.09 \pm 0.99 \pm 0.24$	
4.3874	55.57	28.72	20.24	11.07	8.06	$2.82^{+1.31}_{-1.07}$	$3.99^{+1.86}_{-1.51}$	$0.65^{+0.30}_{-0.24}$	$0.88^{+0.41}_{-0.34}$	1.165	1.051	$8.70^{+4.06}_{-3.29} \pm 0.34$	14.88
4.3965	507.8	28.72	20.40	10.81	7.83	19.39 ± 3.08	27.26 ± 4.33	4.28 ± 0.68	5.89 ± 0.94	1.174	1.051	$6.45 \pm 1.02 \pm 0.26$	
4.4156	1090.7	27.71	19.42	10.42	7.53	37.36 ± 4.23	53.23 ± 6.03	8.33 ± 0.94	11.51 ± 1.30	1.240	1.052	$5.74 \pm 0.65 \pm 0.23$	
4.4362	569.9	25.48	18.08	9.35	6.74	12.15 ± 2.55	17.10 ± 3.58	2.60 ± 0.55	3.61 ± 0.76	1.391	1.054	$3.42 \pm 0.72 \pm 0.14$	
4.4671	111.09	19.78	13.98	7.10	5.12	$-0.35^{+0.89}_{-0.60}$	$-0.50^{+1.26}_{-0.85}$	$-0.07^{+0.19}_{-0.13}$	$-0.10^{+0.26}_{-0.18}$	1.836	1.055	$-0.50^{+0.72}_{-0.85} \pm 0.02$	2.41

(Table continued)

TABLE III. (Continued)

\sqrt{s} (GeV)	\mathcal{L} (pb $^{-1}$)	$\epsilon(\%)^a$	$\epsilon(\%)^b$	$\epsilon(\%)^c$	$\epsilon(\%)^d$	N_{sig}^a	N_{sig}^b	N_{sig}^c	N_{sig}^d	$1 + \delta^{\text{ISR}}$	$\frac{1}{ 1-\eta ^2}$	σ (pb)	σ^{UL} (pb)
4.5271	112.12	7.44	5.18	2.48	1.80	$0.31^{+0.90}_{-0.66}$	$0.44^{+1.30}_{-0.95}$	$0.06^{+0.18}_{-0.13}$	$0.08^{+0.25}_{-0.18}$	5.347	1.054	$0.40^{+1.17}_{-0.86} \pm 0.02$	2.59
4.5745	48.93	1.23	0.85	0.37	0.27	$-0.23^{+0.65}_{-0.40}$	$-0.34^{+0.95}_{-0.57}$	$-0.04^{+0.12}_{-0.07}$	$-0.06^{+0.16}_{-0.10}$	43.404	1.055	$-0.52^{+1.46}_{-0.89} \pm 0.08$	3.28
4.5995	586.9	0.18	0.12	0.04	0.03	$-2.32^{+1.30}_{-1.01}$	$-3.53^{+1.97}_{-1.55}$	$-0.29^{+0.16}_{-0.13}$	$-0.40^{+0.22}_{-0.17}$	19424.100	1.055	$-0.007^{+0.004}_{-0.003} \pm 0.00$	0.01
4.6119	103.83	0.21	0.13	0.05	0.03	$0.01^{+0.71}_{-0.47}$	$0.02^{+1.15}_{-0.77}$	$0.00^{+0.10}_{-0.07}$	$0.00^{+0.14}_{-0.10}$	276.006	1.055	$0.01^{+0.77}_{-0.52} \pm 0.00$	1.78
4.6280	521.52	0.64	0.45	0.19	0.14	$2.24^{+1.90}_{-1.65}$	$3.18^{+2.71}_{-2.34}$	$0.41^{+0.35}_{-0.30}$	$0.55^{+0.47}_{-0.41}$	48.808	1.054	$0.79^{+0.68}_{-0.58} \pm 0.04$	1.82
4.6409	552.41	1.31	0.92	0.40	0.29	$-1.10^{+1.59}_{-1.29}$	$-1.58^{+2.28}_{-1.85}$	$-0.20^{+0.29}_{-0.23}$	$-0.27^{+0.40}_{-0.32}$	23.729	1.054	$-0.37^{+0.53}_{-0.43} \pm 0.02$	0.84
4.6612	529.63	2.68	1.93	0.82	0.61	$0.37^{+1.62}_{-1.36}$	$0.51^{+2.23}_{-1.87}$	$0.07^{+0.29}_{-0.24}$	$0.09^{+0.39}_{-0.33}$	11.549	1.054	$0.12^{+0.55}_{-0.46} \pm 0.00$	1.09
4.6819	1669.31	4.49	3.15	1.35	0.97	$3.15^{+3.10}_{-2.82}$	$4.48^{+4.41}_{-4.01}$	$0.56^{+0.55}_{-0.50}$	$0.77^{+0.76}_{-0.69}$	7.118	1.054	$0.34^{+0.33}_{-0.30} \pm 0.01$	0.83
4.6988	536.45	6.08	4.20	1.77	1.30	$-0.04^{+1.66}_{-1.37}$	$-0.05^{+2.40}_{-1.97}$	$-0.01^{+0.30}_{-0.24}$	$-0.01^{+0.40}_{-0.33}$	5.345	1.055	$-0.01^{+0.56}_{-0.46} \pm 0.00$	1.03
4.7397	164.27	9.85	6.92	2.84	2.02	$0.19^{+0.84}_{-0.60}$	$0.28^{+1.19}_{-0.85}$	$0.03^{+0.14}_{-0.10}$	$0.05^{+0.20}_{-0.14}$	3.335	1.055	$0.21^{+0.89}_{-0.63} \pm 0.01$	1.94
4.7501	367.21	10.85	7.63	3.04	2.23	$1.31^{+1.61}_{-1.35}$	$1.87^{+2.29}_{-1.91}$	$0.22^{+0.27}_{-0.23}$	$0.30^{+0.37}_{-0.31}$	3.046	1.055	$0.62^{+0.76}_{-0.64} \pm 0.02$	1.83
4.7805	512.78	13.34	9.45	3.67	2.68	$-2.54^{+1.30}_{-0.93}$	$-3.59^{+1.83}_{-1.32}$	$-0.41^{+0.21}_{-0.15}$	$-0.57^{+0.29}_{-0.21}$	2.488	1.055	$-0.85^{+0.43}_{-0.31} \pm 0.03$	0.60
4.8431	527.29	17.72	12.67	4.57	3.32	$0.98^{+1.62}_{-1.36}$	$1.37^{+2.27}_{-1.90}$	$0.15^{+0.24}_{-0.21}$	$0.20^{+0.34}_{-0.28}$	1.889	1.056	$0.31^{+0.52}_{-0.43} \pm 0.01$	1.16
4.9180	208.11	21.37	15.16	4.98	3.68	$2.69^{+1.35}_{-1.10}$	$3.79^{+1.90}_{-1.54}$	$0.38^{+0.19}_{-0.15}$	$0.51^{+0.25}_{-0.21}$	1.575	1.056	$2.18^{+1.09}_{-0.89} \pm 0.08$	3.86
4.9509	160.37	22.31	15.89	5.04	3.63	$1.03^{+1.14}_{-0.87}$	$1.44^{+1.60}_{-1.22}$	$0.13^{+0.15}_{-0.11}$	$0.19^{+0.21}_{-0.16}$	1.496	1.056	$1.08^{+1.21}_{-0.92} \pm 0.04$	3.11

^a $J/\psi \rightarrow \mu^+\mu^-$, $\eta \rightarrow \gamma\gamma$.^b $J/\psi \rightarrow e^+e^-$, $\eta \rightarrow \gamma\gamma$.^c $J/\psi \rightarrow \mu^+\mu^-$, $\eta \rightarrow \pi^0\pi^+\pi^-$.^d $J/\psi \rightarrow e^+e^-$, $\eta \rightarrow \pi^0\pi^+\pi^-$.

TABLE IV. Relative systematic uncertainties (%) in the Born cross section measurement. The sources with “**” are the common systematic uncertainties for different c.m. energies. The items with the symbol “†” are estimated with the data sample with the highest statistics ($\sqrt{s} = 4.226$ GeV). The systematic uncertainties include Luminosity (\mathcal{L}_{int}), Branching fraction (\mathcal{B}), ISR correction, γ detection, Tracking ($\mu^+\mu^-/e^+e^-$) (Track1), Tracking ($\pi^+\pi^-$) (Track2), Lepton pair mass window $M(\ell^+\ell^-)$, Kinematic fit, Photon-energy criteria (E_γ), Fit (including background shape, fit range and signal shape), and Others.

\sqrt{s} (GeV)	$\mathcal{L}_{\text{int}}^*$	\mathcal{B}^*	ISR correction	γ detection*†	Track1*	Track2*	$M(\ell^+\ell^-)^\dagger$	Kinematic fit†	E_γ	Fit†	Others*	Total
3.8077	1.0	0.9	0.5	2.0	2.0	0.4	0.1	0.8	1.2	1.0	1.0	3.8
3.8694	1.0	0.9	0.5	2.0	2.0	0.9	0.1	0.8	1.2	1.0	1.0	3.9
3.8962	1.0	0.9	0.5	2.0	2.0	0.5	0.1	0.8	1.2	1.0	1.0	3.8
4.0076	1.0	0.9	0.7	2.0	2.0	0.5	0.1	0.8	1.2	1.0	1.0	3.9
4.0855	1.0	0.9	1.2	2.0	2.0	0.4	0.1	0.8	1.2	1.0	1.0	4.1
4.1285	1.0	0.9	1.1	2.0	2.0	0.5	0.1	0.8	1.2	1.0	1.0	4.0
4.1574	1.0	0.9	0.7	2.0	2.0	0.5	0.1	0.8	1.2	1.0	1.0	3.9
4.1784	1.0	0.9	0.6	2.0	2.0	0.5	0.1	0.8	1.2	1.0	1.0	3.8
4.1888	1.0	0.9	0.6	2.0	2.0	0.5	0.1	0.8	1.2	1.0	1.0	3.8
4.1989	1.0	0.9	0.6	2.0	2.0	0.5	0.1	0.8	1.2	1.0	1.0	3.8
4.2091	1.0	0.9	0.6	2.0	2.0	0.4	0.1	0.8	1.2	1.0	1.0	3.8
4.2186	1.0	0.9	0.6	2.0	2.0	0.4	0.1	0.8	1.2	1.0	1.0	3.9
4.2263	1.0	0.9	0.7	2.0	2.0	0.4	0.1	0.8	1.2	1.0	1.0	3.9
4.2357	1.0	0.9	0.8	2.0	2.0	0.4	0.1	0.8	1.2	1.0	1.0	3.9
4.2436	1.0	0.9	0.9	2.0	2.0	0.5	0.1	0.8	1.2	1.0	1.0	4.0
4.2580	1.0	0.9	1.4	2.0	2.0	0.5	0.1	0.8	1.2	1.0	1.0	4.2
4.2668	1.0	0.9	1.6	2.0	2.0	0.5	0.1	0.8	1.2	1.0	1.0	4.3
4.2777	1.0	0.9	2.2	2.0	2.0	0.5	0.1	0.8	1.2	1.0	1.0	4.6
4.2879	1.0	0.9	2.0	2.0	2.0	0.6	0.1	0.8	1.2	1.0	1.0	4.5
4.3079	1.0	0.9	2.0	2.0	2.0	0.4	0.1	0.8	1.2	1.0	1.0	4.5
4.3121	1.0	0.9	1.7	2.0	2.0	0.6	0.1	0.8	1.2	1.0	1.0	4.3
4.3374	1.0	0.9	1.2	2.0	2.0	0.4	0.1	0.8	1.2	1.0	1.0	4.1
4.3583	1.0	0.9	0.9	2.0	2.0	0.6	0.1	0.8	1.2	1.0	1.0	4.0
4.3774	1.0	0.9	0.9	2.0	2.0	0.5	0.1	0.8	1.2	1.0	1.0	4.0
4.3874	1.0	0.9	0.8	2.0	2.0	0.4	0.1	0.8	1.2	1.0	1.0	3.9
4.3965	1.0	0.9	0.9	2.0	2.0	0.5	0.1	0.8	1.2	1.0	1.0	4.0
4.4156	1.0	0.9	0.9	2.0	2.0	0.5	0.1	0.8	1.2	1.0	1.0	4.0
4.4362	1.0	0.9	1.1	2.0	2.0	0.6	0.1	0.8	1.2	1.0	1.0	4.0
4.4671	1.0	0.9	1.2	2.0	2.0	0.3	0.1	0.8	1.2	1.0	1.0	4.1
4.5271	1.0	0.9	2.1	2.0	2.0	0.3	0.1	0.8	1.2	1.0	1.0	4.5
4.5745	1.0	0.9	14.9	2.0	2.0	0.5	0.1	0.8	1.2	1.0	1.0	15.9
4.5995	1.0	0.9	27.2	2.0	2.0	0.2	0.1	0.8	1.2	1.0	1.0	27.9
4.6119	1.0	0.9	17.9	2.0	2.0	0.5	0.1	0.8	1.2	1.0	1.0	18.8
4.6280	1.0	0.9	2.3	2.0	2.0	0.3	0.1	0.8	1.2	1.0	1.0	4.6
4.6409	1.0	0.9	1.2	2.0	2.0	0.3	0.1	0.8	1.2	1.0	1.0	4.1
4.6612	1.0	0.9	1.0	2.0	2.0	0.3	0.1	0.8	1.2	1.0	1.0	4.0
4.6819	1.0	0.9	0.8	2.0	2.0	0.3	0.1	0.8	1.2	1.0	1.0	3.9
4.6988	1.0	0.9	0.7	2.0	2.0	0.3	0.1	0.8	1.2	1.0	1.0	3.9
4.7397	1.0	0.9	0.6	2.0	2.0	1.0	0.1	0.8	1.2	1.0	1.0	4.0
4.7501	1.0	0.9	0.6	2.0	2.0	0.3	0.1	0.8	1.2	1.0	1.0	3.8
4.7805	1.0	0.9	0.6	2.0	2.0	0.3	0.1	0.8	1.2	1.0	1.0	3.8
4.8431	1.0	0.9	0.6	2.0	2.0	0.3	0.1	0.8	1.2	1.0	1.0	3.8
4.9180	1.0	0.9	0.6	2.0	2.0	0.2	0.1	0.8	1.2	1.0	1.0	3.8
4.9509	1.0	0.9	0.5	2.0	2.0	0.2	0.1	0.8	1.2	1.0	1.0	3.8

(2) *Correlated part*

Considering the correlated systematic uncertainties, which obey a Gaussian distribution, as the nuisance parameter of the overall likelihood function in the line shape fit, the likelihood function of total data samples is defined as

$$L'_{\text{tot}} = \int \left[\prod_{i=1}^{44} L'_i(\sigma_i^{\text{fit}} \cdot \epsilon) \right] \times \text{Gauss}(\epsilon; 1, \epsilon^{\text{corr}}) d\epsilon, \quad (\text{C2})$$

where ϵ^{corr} is the total correlated relative systematic uncertainty. Some correlated uncertainties are different for each energy point; to be conservative, the largest value is used.

Finally, using L'_{tot} to repeat the fit, the differences of the results are considered as the systematic uncertainties from the cross section measurement.

-
- [1] N. Brambilla, S. Eidelman, C. Hanhart, A. Nefediev, C.-P. Shen, C. E. Thomas, A. Vairo, and C.-Z. Yuan, *Phys. Rep.* **873**, 1 (2020).
- [2] B. Aubert *et al.* (BABAR Collaboration), *Phys. Rev. Lett.* **95**, 142001 (2005).
- [3] C. Z. Yuan *et al.* (Belle Collaboration), *Phys. Rev. Lett.* **99**, 182004 (2007).
- [4] J. P. Lees *et al.* (BABAR Collaboration), *Phys. Rev. D* **86**, 051102 (2012).
- [5] Z. Q. Liu *et al.* (Belle Collaboration), *Phys. Rev. Lett.* **110**, 252002 (2013).
- [6] B. Aubert *et al.* (BABAR Collaboration), *Phys. Rev. Lett.* **98**, 212001 (2007).
- [7] J. P. Lees *et al.* (BABAR Collaboration), *Phys. Rev. D* **89**, 111103 (2014).
- [8] X. L. Wang *et al.* (Belle Collaboration), *Phys. Rev. Lett.* **99**, 142002 (2007).
- [9] X. L. Wang *et al.* (Belle Collaboration), *Phys. Rev. D* **91**, 112007 (2015).
- [10] M. Ablikim *et al.* (BESIII Collaboration), *Phys. Rev. Lett.* **118**, 092001 (2017).
- [11] M. Ablikim *et al.* (BESIII Collaboration), *Phys. Rev. D* **106**, 072001 (2022).
- [12] M. Ablikim *et al.* (BESIII Collaboration), *Phys. Rev. D* **102**, 012009 (2020).
- [13] M. Ablikim *et al.* (BESIII Collaboration), *Phys. Rev. D* **107**, 092005 (2023).
- [14] M. Ablikim *et al.* (BESIII Collaboration), *Chin. Phys. C* **46**, 111002 (2022).
- [15] M. Ablikim *et al.* (BESIII Collaboration), *Phys. Rev. D* **96**, 032004 (2017).
- [16] M. Ablikim *et al.* (BESIII Collaboration), *Phys. Rev. D* **104**, 052012 (2021).
- [17] M. Ablikim *et al.* (BESIII Collaboration), *Phys. Rev. Lett.* **118**, 092002 (2017).
- [18] M. Ablikim *et al.* (BESIII Collaboration), *Phys. Rev. Lett.* **114**, 092003 (2015).
- [19] M. Ablikim *et al.* (BESIII Collaboration), *Phys. Rev. D* **99**, 091103 (2019).
- [20] M. Ablikim *et al.* (BESIII Collaboration), *Phys. Rev. Lett.* **122**, 102002 (2019).
- [21] M. Ablikim *et al.* (BESIII Collaboration), *Phys. Rev. Lett.* **129**, 102003 (2022).
- [22] Y.-B. Dong, Y.-W. Yu, Z.-Y. Zhang, and P.-N. Shen, *Phys. Rev. D* **49**, 1642 (1994).
- [23] B.-Q. Li and K.-T. Chao, *Phys. Rev. D* **79**, 094004 (2009).
- [24] D.-Y. Chen, X. Liu, and T. Matsuki, *Phys. Rev. D* **91**, 094023 (2015).
- [25] M. N. Anwar, Y. Lu, and B.-S. Zou, *Phys. Rev. D* **95**, 114031 (2017).
- [26] G. Li and X.-H. Liu, *Phys. Rev. D* **88**, 094008 (2013).
- [27] D.-Y. Chen, C.-J. Xiao, and J. He, *Phys. Rev. D* **96**, 054017 (2017).
- [28] M. Ablikim *et al.* (BESIII Collaboration), *Phys. Rev. D* **102**, 031101 (2020).
- [29] M. Ablikim *et al.* (BESIII Collaboration), *Nucl. Instrum. Methods Phys. Res., Sect. A* **614**, 345 (2010).
- [30] C. Yu *et al.*, in *7th International Particle Accelerator Conference* (2016), p. TUYA01, 10.18429/JACoW-IPAC2016-TUYA01.
- [31] P. Cao *et al.*, *Nucl. Instrum. Methods Phys. Res., Sect. A* **953**, 163053 (2020).
- [32] M. Ablikim *et al.* (BESIII Collaboration), *Chin. Phys. C* **40**, 063001 (2016).
- [33] M. Ablikim *et al.* (BESIII Collaboration), *Chin. Phys. C* **45**, 103001 (2021).
- [34] M. Ablikim *et al.* (BESIII Collaboration), *Chin. Phys. C* **46**, 113003 (2022).
- [35] M. Ablikim *et al.* (BESIII Collaboration), *Chin. Phys. C* **39**, 093001 (2015).
- [36] M. Ablikim *et al.* (BESIII Collaboration), *Chin. Phys. C* **46**, 113002 (2022).
- [37] S. Agostinelli *et al.* (GEANT4 Collaboration), *Nucl. Instrum. Methods Phys. Res., Sect. A* **506**, 250 (2003).
- [38] K.-X. Huang, Z.-J. Li, Z. Qian, J. Zhu, H.-Y. Li, Y.-M. Zhang, S.-S. Sun, and Z.-Y. You, *Nucl. Sci. Tech.* **33**, 142 (2022).
- [39] S. Jadach, B. F. L. Ward, and Z. Was, *Comput. Phys. Commun.* **130**, 260 (2000).
- [40] S. Jadach, B. F. L. Ward, and Z. Was, *Phys. Rev. D* **63**, 113009 (2001).
- [41] D. J. Lange, *Nucl. Instrum. Methods Phys. Res., Sect. A* **462**, 152 (2001).
- [42] R.-G. Ping, *Chin. Phys. C* **32**, 599 (2008).
- [43] R. L. Workman *et al.* (Particle Data Group), *Prog. Theor. Exp. Phys.* **2022**, 083C01 (2022).

- [44] J. C. Chen, G. S. Huang, X. R. Qi, D. H. Zhang, and Y. S. Zhu, *Phys. Rev. D* **62**, 034003 (2000).
- [45] R.-L. Yang, R.-G. Ping, and H. Chen, *Chin. Phys. Lett.* **31**, 061301 (2014).
- [46] R.-G. Ping, *Chin. Phys. C* **38**, 083001 (2014).
- [47] F. Campanario, H. Czyz, J. Gluza, T. Jeliński, G. Rodrigo, S. Tracz, and D. Zhuridov, *Phys. Rev. D* **100**, 076004 (2019).
- [48] E. Richter-Was, *Phys. Lett. B* **303**, 163 (1993).
- [49] S. Actis *et al.* (Working Group on Radiative Corrections, Monte Carlo Generators for Low Energies Collaboration), *Eur. Phys. J. C* **66**, 585 (2010).
- [50] W. Sun, T. Liu, M. Jing, L. Wang, B. Zhong, and W. Song, *Front. Phys.* **16**, 64501 (2021).
- [51] M. Ablikim *et al.* (BESIII Collaboration), *Phys. Rev. D* **86**, 071101 (2012).
- [52] M. Ablikim *et al.* (BESIII Collaboration), *Phys. Rev. D* **91**, 112005 (2015).
- [53] X. L. Wang, Y. L. Han, C. Z. Yuan, C. P. Shen, and P. Wang (Belle Collaboration), *Phys. Rev. D* **87**, 051101 (2013).
- [54] S. X. Li *et al.*, *Phys. Rev. D* **103**, 072004 (2021).
- [55] K. S. Cranmer, *Comput. Phys. Commun.* **136**, 198 (2001).
- [56] X.-X. Liu, X.-R. Lü, and Y.-S. Zhu, *Chin. Phys. C* **39**, 103001 (2015).
- [57] K. Stenson, arXiv:physics/0605236.
- [58] Y. Bai and D.-Y. Chen, *Phys. Rev. D* **99**, 072007 (2019).
- [59] M. Ablikim *et al.* (BESIII Collaboration), *Phys. Rev. Lett.* **110**, 252001 (2013).
- [60] M. Ablikim *et al.* (BESIII Collaboration), *Phys. Rev. D* **99**, 032001 (2019).
- [61] M. Ablikim *et al.* (BESIII Collaboration), *Phys. Rev. D* **81**, 052005 (2010).
- [62] M. Ablikim *et al.* (BESIII Collaboration), *Phys. Rev. D* **87**, 012002 (2013).
- [63] R. Barlow, arXiv:hep-ex/0207026.
- [64] M. Ablikim *et al.* (BESIII Collaboration), *Nature (London)* **606**, 64 (2022).
- [65] E. V. Abakumova *et al.*, *Nucl. Instrum. Methods Phys. Res., Sect. A* **659**, 21 (2011).